Basin Research

IAS EAGE

Basin Research (2014) **0**, 1–25, doi: 10.1111/bre.12069

Late Miocene to Pliocene stratigraphy of the Kura Basin, a subbasin of the South Caspian Basin: implications for the diachroneity of stage boundaries

Adam M. Forte,*,† Dawn Y. Sumner,* Eric Cowgill,* Marius Stoica,‡ Ibrahim Murtuzayev,§ Talat Kangarli,§ Mikheil Elashvili,¶ Tea Godoladze¶ and Zurab Javakhishvili¶

**Department of Geology, University of California, Davis, CA, USA*
†*School of Earth and Space Exploration, Arizona State University, Tempe, AZ, USA*
‡*University of Bucharest, Bucharest, Romania*
§*Geological Institute of Azerbaijan, Baku, Azerbaijan*
¶*Ilia State University, Tbilisi, Georgia*

ABSTRACT

Relative ages of late Cenozoic stratigraphy throughout the Caspian region are referenced to regional stages that are defined by changes in microfauna and associated extreme (>1000 m) variations in Caspian base level. However, the absolute ages of these stage boundaries may be significantly diachronous because many are based on the first occurrence of either transgressive or regressive facies, the temporal occurrence of which should depend on position within a basin. Here, we estimate the degree of diachroneity along the Akchagyl regional stage boundary within the Caspian basin system by presenting two late Miocene–Pliocene aged measured sections, Sarica and Vashlovani, separated by 50 km and exposed within the Kura fold-thrust belt in the interior of the Kura Basin. The Kura Basin is a western subbasin of the South Caspian Basin and the sections presented here are located >250 km from the modern Caspian coast. New U–Pb detrital zircon ages from the Sarica section constrain the maximum depositional age for Productive Series strata, a lithostratigraphic package considered correlative with the 2–3 Myr-long regional Eoakchagylian or Kimmerian stage that corresponds to a period of extremely low (>500 m below the modern level) Caspian base level. This new maximum depositional age from the Productive Series at Sarica of 2.5 ± 0.2 Ma indicates that the regionally extensive Akchagyl transgression, which ended the deposition of the Productive Series near the Caspian coast at 3.2 Ma, may have appeared a minimum of 0.5 Myr later in the northern interior of the Kura Basin than at the modern Caspian Sea coast. The results of this work have important implications for the tectonic and stratigraphic history of the region, suggesting that the initiation of the Plio–Pleistocene Kura fold-thrust belt may have not been as diachronous along strike as previously hypothesized. More generally, these results also provide a measure of the magnitude of diachroneity possible along sequence boundaries, particularly in isolated basins. Comparison of accumulation rates between units in the interior of the Kura subbasin and the South Caspian main basin suggest that extremely large variations in these rates within low-stand deposits may be important in identifying the presence of subbasins in older stratigraphic packages.

INTRODUCTION

Sequence stratigraphy has proven invaluable both as a conceptual framework for understanding the response of depositional systems to changes in base level, but also as a tool for correlating disparate parts of those depositional systems (e.g. van Hinte, 1978; Steenwinkel, 1990; Van Wagoner & Bertram, 1995; Catuneanu, 2002). Of particular importance for the latter has been a concerted effort to understand the extent to which sequence boundaries represent isochronous or diachronous geologic or hydrological events (e.g. Carter *et al.*, 1998; Catuneanu *et al.*, 1998; Liu *et al.*, 1998; Strong & Paola, 2008; Martin *et al.*, 2009). Generally, modelling indicates that both regressive and transgressive surfaces are diachronous, but that transgressive surfaces tend to be less so and can sometimes be nearly isochronous (e.g. Strong & Paola, 2008;

Correspondence: Adam M. Forte, School of Earth and Space Exploration, Arizona State University, ISTB4, 781 E. Terrace Road, Tempe, AZ 85287-6004, USA. Email: amforte@ucdavis.edu

Bhattacharya, 2011). In detail, first transgressive surfaces, which form the lower boundaries of transgressive systems tracts, are necessarily diachronous, but maximum flooding surfaces are typically argued to represent nearly isochronous time lines within a basin (Mancini & Tew, 1997).

However, the diachroneity of sequence boundaries is highly influenced by local effects, such as the rate of sediment supply and generation of accommodation space (e.g. Allen & Johnson, 2011). This is particularly apparent in the stratigraphic records of basins fringed by one or more subbasins (e.g. Brown *et al.*, 2005; Munteanu *et al.*, 2012) as packages which represent maximum flooding surfaces in the main basin may represent first transgressive surfaces in subbasins. This enhanced diachroneity results primarily from differential bathymetry and topography between the main and subbasins that cause changes in base level to affect different parts of the basin system at different times (e.g. Liu *et al.*, 1998). An additional important process is the tendency for the main locus of deposition to shift during base-level variations (e.g. Munteanu *et al.*, 2012). For example, as base-level rises and a subbasin is inundated, it transitions from a sediment source to a sediment sink and introduces a sudden, large increase in accommodation space that tends to shift the main depocentre to the subbasin and effectively starve the main basin of sediment (Munteanu *et al.*, 2012). Thus, in systems characterized by main and subbasin pairs, the maximum flooding surface may not be a continuous, nearly isochronous deposit because at the time of maximum flooding, the main basin may experience a period of nondeposition as sediment is sequestered in the subbasin. Complications such as this have led workers to suggest that it may be necessary to develop separate chronologies and stratigraphic frameworks between main basins and subbasins (Brown *et al.*, 2005). Ultimately, understanding and measuring the degree of diachroneity of sequence boundaries and maximum flooding surfaces throughout basin systems has important implications for interpreting the stratigraphic fill of these basins because the boundaries are coincident with abrupt facies transitions commonly used to define stratigraphic units and formations (Bhattacharya, 2011).

Much of our understanding of the diachronous nature of sequence boundaries and flooding surfaces comes from models of depositional systems (e.g. Catuneanu *et al.*, 1998; Liu *et al.*, 2004; Strong & Paola, 2008; Martin *et al.*, 2009), which unfortunately do not provide absolute constraints on the magnitude of diachroneity possible within sequence stratigraphic surfaces. The Paratethyan basins present an interesting venue in which to address this problem by using field studies to explore the diachroneity of sequence stratigraphic surfaces and stage boundaries. These basins span Eastern Europe to Central Asia (Fig. 1), have a complicated history of interconnection, are characterized by relatively large changes in base level during periods of isolation (e.g. Zubakov, 2001; Popov *et al.*, 2010), and have multiple hierarchies of basins and subbasins. For example, the Pannonian Basin is a subbasin with respect to the Dacian Basin, which in turn is a subbasin with respect to the Black Sea (Fig. 1a). The Black Sea and Dacian basin–subbasin pair is relatively well studied and contains evidence of both depocentre migration from the main basin (Black Sea) to the subbasin (Dacian) during transgressions (Munteanu *et al.*, 2012) and diachronous stage boundaries (e.g. Vasiliev *et al.*, 2004; Krijgsman *et al.*, 2010; Stoica *et al.*, 2013).

Of the Paratethyan basins, the Caspian Sea has experienced some of the longest periods of isolation and most extreme variations in base level (e.g. Zubakov, 2001; Forte & Cowgill, 2013) due to its distal position relative to the open ocean. Of particular interest is the transition between the Productive Series and Akchagyl regional stages, which represent one of the largest transgressions ever documented on Earth, during which the base level of the Caspian rose from between 600 and 1500 m below its current level (e.g. Reynolds *et al.*, 1998; Zubakov, 2001; Green *et al.*, 2009) to between 60 and 200 m above its current level (Figs 1a and 2, e.g. Kvasov, 1964; Zubakov, 1992; Jones & Simmons, 1996).

In the Caspian system, the main basin is the South Caspian Basin, which is fringed by multiple subbasins (Fig. 1a). Of these different subbasins, the Kura Basin, which lies to the west of the South Caspian, provides a unique opportunity to explore the dynamics of depositional shifts, because large portions of the sedimentary fill of this basin are now exposed in the Plio–Pleistocene Kura fold–thrust belt, which is actively forming along the southeastern margin of the Greater Caucasus Mountains (Forte *et al.*, 2010, 2013). Previous coarse resolution mapping (1 : 200 000–1 : 1 000 000 scale) indicates that the sediments exposed in this fold–thrust belt are predominantly late Cenozoic strata (e.g. Abdullaev *et al.*, 1957; Nalivkin, 1976; Gudjabidze, 2003; Ali-Zade, 2005) deposited coevally with many of the extreme variations in Caspian base level (e.g. Zubakov, 2001; Popov *et al.*, 2010; Forte & Cowgill, 2013). Because regional stage boundaries in the Caspian region are primarily based on the variations of Caspian base level (e.g. Zubakov & Borzenkova, 1990; Jones & Simmons, 1996; Forte & Cowgill, 2013) they are analogous to sequence boundaries defined on the basis of eustatic sea level variations. Thus, correlating strata and regional stages boundaries between the Kura Basin and the South Caspian should help quantify the absolute amounts of time represented in some diachronous sequence stratigraphic surfaces.

Although the late Cenozoic stratigraphy of the South Caspian basin is relatively well described, (e.g. Inan *et al.*, 1997; Reynolds *et al.*, 1998; Devlin *et al.*, 1999; Hinds *et al.*, 2004; Aliyeva, 2005; Kroonenberg *et al.*, 2005; Abreu & Nummedal, 2007; Green *et al.*, 2009; Vincent *et al.*, 2010; van Baak *et al.*, 2013) the Miocene–Pliocene stratigraphy of the Kura Basin is only described in general summary works (e.g. Shirinov & Bajenov, 1962;

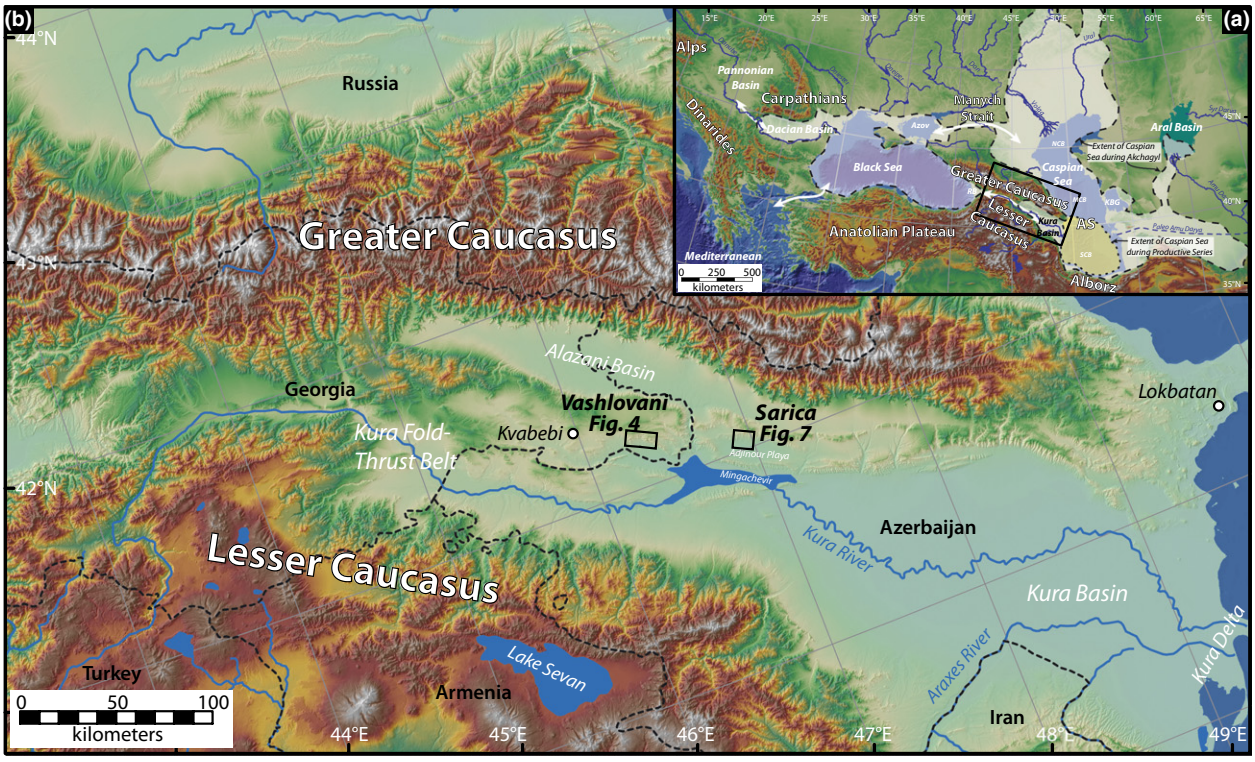

Fig. 1. (a) Map showing the distribution of Paratethyan Basins and highlighting some of the main physiographic regions discussed in the text. Short dashed black lines show the estimated shorelines for the Caspian during the Productive Series regression (Reynolds *et al.*, 1998) and long dashed lines outline the Akchagylian transgression (Popov *et al.*, 2006). Thick white lines show approximate positions of spill points, or 'gateways', between different Paratethyan Basins. AS, Apsheron Sill; SCB, South Caspian Basin; MCB, Middle Caspian Basin; NCB, North Caspian Basin; and KBG, Kara-Bogaz-Gol. Black box represents the extent of (b). Figure modified from Forte & Cowgill (2013). (b) Regional location map for the two measured sections in this study, Vashlovani and Sarica, and two previously published sections described in the text, Lokbatan (e.g. van Baak *et al.*, 2013) and Kvabebi (Agustí *et al.*, 2009). Boxes outline detailed maps for Vashlovani in Fig. 4 and Sarica in Fig. 7.

Mamedov, 1973; Nalivkin, 1973). Detailed local descriptions within the Kura Basin are generally lacking, as are clear assessments of the absolute age of the stratigraphy, largely precluding the use of this prior work in better understanding the extent to which sequence stratigraphic and regional stage boundaries are diachronous. To address this problem, we present two new measured sections in the interior of the Kura Basin, the Vashlovani and Sarica sections, which are located in the Kura fold-thrust belt and expose late Cenozoic stratigraphy deposited coevally with many of the extremely large base-level variations within the Caspian Sea and growth of the Greater Caucasus Mountains (Fig. 1a). Here, we provide descriptions of these sections and focus on correlating them to the regional Caspian stages in a sequence stratigraphic framework, however it should be emphasized that the analysis presented here is largely of a reconnaissance nature and represents some of the first stratigraphic work to be published within this interior portion of the Greater Caucasus foreland basin. Where possible, we also incorporate our new biostratigraphic results and U-Pb ages of detrital zircons to constrain maximum depositional ages to explore both the late Cenozoic stratigraphic architecture of the northern Kura Basin and the potential diachroneity of stage boundaries between the Kura subbasin and main South Caspian Basin.

KURA BASIN CHRONOSTRATIGRAPHIC FRAMEWORK

Previous work investigating the Cenozoic stratigraphy of the Kura Basin was done within the chronostratigraphic framework constructed from fluctuations in the base level of the Caspian and related changes in biostratigraphic assemblages (e.g. Shirinov & Bajenov, 1962; Mamedov, 1973; Nalivkin, 1973; Zubakov & Borzenkova, 1990; Jones & Simmons, 1996; Forte & Cowgill, 2013). In detail, the definition of the absolute age of stage boundaries, the geological significance of the stages, and their correlation with the global geologic time scale have all proven problematic. The controversial nature of these stages stem from several key factors, including: (1) The endemic nature of nearly all organisms used for biostratigraphic divisions (e.g. Menabde *et al.*, 1993; Jones & Simmons, 1996; Dumont, 1998; Boomer *et al.*, 2010); (2) A complicated history of variable interconnection of the Caspian with other Paratethyan basins, the Mediterranean and the

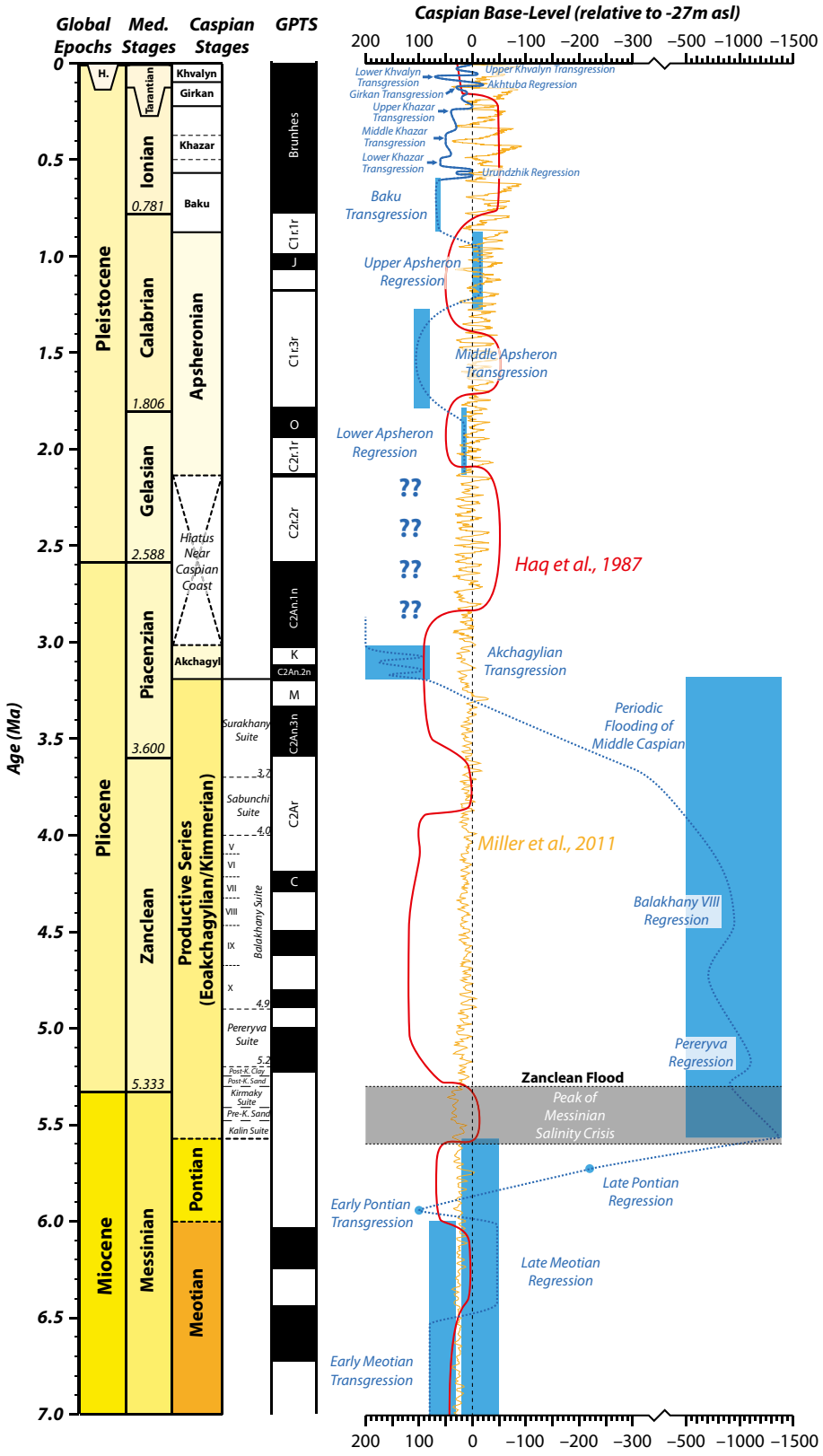

Fig. 2. Chronostratigraphic framework and reconstructed Caspian base level from 7 Ma to present (after Forte & Cowgill, 2013). Absolute ages of boundaries for the global epochs, Mediterranean stages and global palaeomagnetic time scale (GPTS) are from Gradstein *et al.* (2012). Absolute ages of boundaries for Caspian stages (i.e. the regional time scale) are taken from van Baak *et al.* (2013) and are principally defined from dating in the Lokbatan section (see Fig. 1). Red eustatic sea level curve is from Haq *et al.* (1987) and orange eustatic sea level curve is from Miller *et al.* (2011). Blue bars, dots and dashed lines indicate approximate elevations of Caspian base level compiled by Forte & Cowgill (2013). Uncertainty in the base level history between the Akchagyl and the Lower Apsheron regional stages during the hiatus in deposition at Lokbatan are represented by the '??', see Forte & Cowgill (2013) for further discussion.

global ocean (e.g. Zubakov, 1992; Svitoch, 1999; Svitoch *et al.*, 2000; Popov *et al.*, 2006; Vasiliev *et al.*, 2010); (3) The potential for large variations in Caspian base level that are in the order of magnitude larger than those observed in the global ocean (Fig. 2, see reviews by Zubakov, 2001; Popov *et al.*, 2010; Forte & Cowgill, 2013); (4) The rapid and chaotic variations of Caspian base level during periods of isolation (e.g. Kroonenberg *et al.*, 1997; Mamedov, 1997; Rychagov, 1997; Sedletskii & Baikov, 1997; Kozhevnikova & Shveikina, 2008; Rumyantsev *et al.*, 2008); and (5) An unclear primary driving mechanism for the hydrology of the Caspian Basin (e.g. Kvasov, 1983; Zubakov, 1988; Kizlov & Toropov, 2007; Forte & Cowgill, 2013).

In detail, the history of Caspian base level variations upon which the regional time scale is based, have been variably reported, with attempts to relate changes in the Caspian to variations in the global ocean (Jones & Simmons, 1996), the Mediterranean Sea (Zubakov, 2001) or the Black Sea (Popov *et al.*, 2010). The geologic record of variation in Caspian base level is relatively well preserved into the early Miocene in the architecture of deltaic strata (e.g. Kroonenberg *et al.*, 1997; Overeem *et al.*, 2003a,b; Hoogendoorn *et al.*, 2005; Kroonenberg *et al.*, 2005), distribution of lacustrine deposits (e.g. Zubakov, 1992; Mamedov, 1997) and flights of river terraces and palaeoshorelines extending more than 500 km into northern Eurasia (e.g. Svitoch, 1999; Matoshko *et al.*, 2004). Recently, Forte & Cowgill (2013) synthesized these disparate primary data sources and previous estimates of Caspian base level in an attempt to present a more complete view of the late Miocene to present Caspian base level history and the uncertainty associated with that history (Fig. 2). Here, we use that new regional synthesis to facilitate stratigraphic correlation within the Kura Basin.

Ongoing efforts to better constrain the absolute ages of the stage boundaries throughout the former Paratethyan basins integrate detailed magnetostratigraphic, biostratigraphic and geochronologic studies to correlate these boundaries to the global geologic time scale (e.g. Vasiliev *et al.*, 2004, 2005; Krijgsman *et al.*, 2010; van Baak *et al.*, 2013). These recent studies indicate that some of the stage boundaries are nonsynchronous in the various Paratethyan basins and in some cases may not track the same hydrological event between different basins (e.g. Vasiliev *et al.*, 2004; Krijgsman *et al.*, 2010; Stoica *et al.*, 2013). Here, we primarily use the ages of regional stage boundaries from the Lokbatan section on the Apsheron Peninsula of eastern Azerbaijan, which were determined by a combination of magnetostratigraphic, biostratigraphic and geochronologic data (Fig. 1, van Baak *et al.*, 2013). Because this section is located adjacent to the modern day Caspian Sea coast, the ages of the stage boundaries here are good first-order approximations for the Caspian Sea region. However, it is important to note that the ages for the stage boundaries used here are the preferred options presented by van Baak *et al.* (2013), although as described in the original publication, significant uncertainty remains in these correlations. Additionally, although the Lokbatan section is generally a high fidelity record, it does contain hiatuses, such as an *ca.* 0.9-Myr-long gap between the Akchagyl and the overlying Apsheron stage, attributed to initiation of deformation in the Lokbatan area (Fig. 2, e.g. van Baak *et al.*, 2013).

For the Vashlovani and Sarica sections, we are principally concerned with the Meotian, Pontian, Productive Series (considered correlative with the Eoakchagylian stage in the Caspian Sea and the Kimmerian stage in the Black Sea), Akchagyl and Apsheron regional stages (Fig. 2). During the Meotian and Pontian stages, the Caspian was intermittently connected to the Black and Mediterranean Sea and Caspian base level generally fluctuated within 100 m of the modern base level (Fig 2., e.g. Popov *et al.*, 2006; Forte & Cowgill, 2013). Deposition of the Productive Series corresponds to an extremely low period of base level, with estimates ranging from 600 to 1500 m below the modern level (Fig 2, e.g. Forte & Cowgill, 2013 and references therein). This dramatic drop in base level drove incision and formation of large palaeo-canyons exceeding 600 m in depth along the Kura, Volga and palaeo-Amu-Darya rivers (Fig. 1, e.g. Kroonenberg *et al.*, 2005). Deposition of the Productive Series ended with the Akchagyl regional stage, corresponding to an apparently abrupt rise in Caspian base level, reaching a maximum of 200 m above the modern level (Fig 2, e.g. Forte & Cowgill, 2013 and references therein). The younger Apsheron regional stage represents a return to lower, but significantly more variable Caspian base level (Fig 2., e.g. Forte & Cowgill, 2013 and references therein).

FIELD AND CORRELATION METHODS

For the two measured sections, we logged grain size, sorting, sedimentary structures and changes in lithology at the decimetre scale over the course of two field seasons. Generally, observations were limited to the line of section, but some strata of particular interest were traced laterally in the field. In addition, when possible, large (>100 m thick) and distinctive lithologic packages were traced in Google Earth imagery using colour and outcrop style to further assess the lateral continuity of the strata. In the Sarica section, palaeocurrents were estimated by measuring the orientation of imbricated clasts within conglomerate. In all sections, sandstone samples were collected for reconnaissance provenance analysis, utilizing petrography, geochemistry and U-Pb dating of detrital zircons. The majority of these provenance results are presented in a preliminary form elsewhere (Forte, 2012). We use limited results from the geochemical and petrographic data aid in the interpretation of depositional environments of one unit within Vashlovani (Unit V2), and subsets of U-Pb ages of detrital zircons to constrain maximum depositional ages for one unit within Sarica (Unit S1) and one unit within Vashlovani (Unit V3). The sampling strategy for these sandstones emphasized collecting samples from

distinct lithologic packages at the expense of evenly spaced samples. Because of the poor induration of most outcrops and to assure collection of an uncontaminated or relatively unweathered sample, preference was given for well-indurated units during sample collection. In this work, we only present partial detrital zircon results from two samples, as the full datasets will be presented in a forthcoming publication. We also collected mudstone samples for micropalaeontological analyses. The micropalaeontological assessment focuses on ostracods, with additional data derived from forams, mollusks and gastropods. Methods employed for the preparation of micropalaeontology samples and the correlation between specific faunal assemblages and regional stages are described in detail by van Baak *et al.* (2013) and Stoica *et al.* (2013).

We defined and described four litho-facies (e.g. Miall, 1977), and then assigned one to each stratigraphic interval. The defined litho-facies are unlaminated silt and clay, massive silt, cross-stratified sand and gravel, and massive gravel facies (Table 1 and Fig. 3). Detailed descriptions of litho-facies characteristics are included in the supplemental material (Appendix S1). We used the distributions of these facies to define stratigraphic units within each section. We then used the litho-facies and micropalaeontological results to interpret the broad depositional setting for each stratigraphic unit. Finally, we interpreted these long-term trends in environments in the context of changes in regional base level and correlated these inferred changes to the newly assembled Caspian base level curve (Fig. 2, Forte & Cowgill, 2013). For a more complete description of Caspian base level history, the data supporting this reconstruction, driving mechanisms behind the variations, and an assessment of the uncertainties, see Forte & Cowgill (2013).

RESULTS: KURA BASIN STRATIGRAPHY

The two new stratigraphic sections, Vashlovani and Sarica, are exposed within the Kura fold-thrust belt along the northern margin of the Kura Basin in Georgia and Azerbaijan (Fig. 1b; Table 2). In the following descriptions, positions within the measured sections are given in metres relative to the base of the section.

Vashlovani

The Vashlovani section is 1475 m thick and is located in the Vashlovani Nature Reserve in southeastern Georgia (Figs 1 and 4; Table 2). The section was measured within the southern portion of the Pantishara Gorge, which was previously mapped as Meotian–Pontian sediments unconformably overlain by Akchagyl- and Apsheron-aged strata (Fig. 4, Abdullaev *et al.*, 1957; Gudjabidze, 2003). We divide this section into three stratigraphic units, V1, V2 and V3 (Fig. 5).

Table 1. Litho-facies

Facies name	Grainsize	Sedimentary structures	Colour	Fossils	Inferred environment
Unlaminated silt and clay facies	Clay and silt with greater than 10% silt	Rare mm-scale interbeds of silts and clays Coal seams, roots, and rhizoliths Mud cracks	Clayey-silt (10–50% silt): tan-grey mottled Silty clay: (50–90% silt): tan to buff	Bivalves and gastropods common Leaf impressions	Shallow ephemeral ponds or lakes
Massive silt facies	Silt and fine sand	Centimetre-scale interbeds of laminated silt and clay	Tan to buff	Rare to absent fossils	Floodplain deposits
Cross-stratified sand and gravel facies	Sand with isolated conglomerate	Often have scours at base Trough cross-bedding, planar cross-stratification, and lenses of fossil concentrations	Tan to brown Isolated packages with distinctive iron staining and dark red colour	Intact fossils rare, abundant fossil concentrations with fragmented skeletal material Mammalian fossils Woody debris	Fluvial Channel, either meandering or anastomosing braded rivers
Massive gravel facies	Conglomerate (pebble to boulder) with isolated sand bodies	Often have scoured bases with decimetre scale relief Occasional mud clasts near base	Brown to dark brown	Rare to absent fossils	Braided fluvial or alluvial fan

Litho-faces for the northern Kura Basin. See Appendix S1 for more detailed descriptions of facies characteristics.

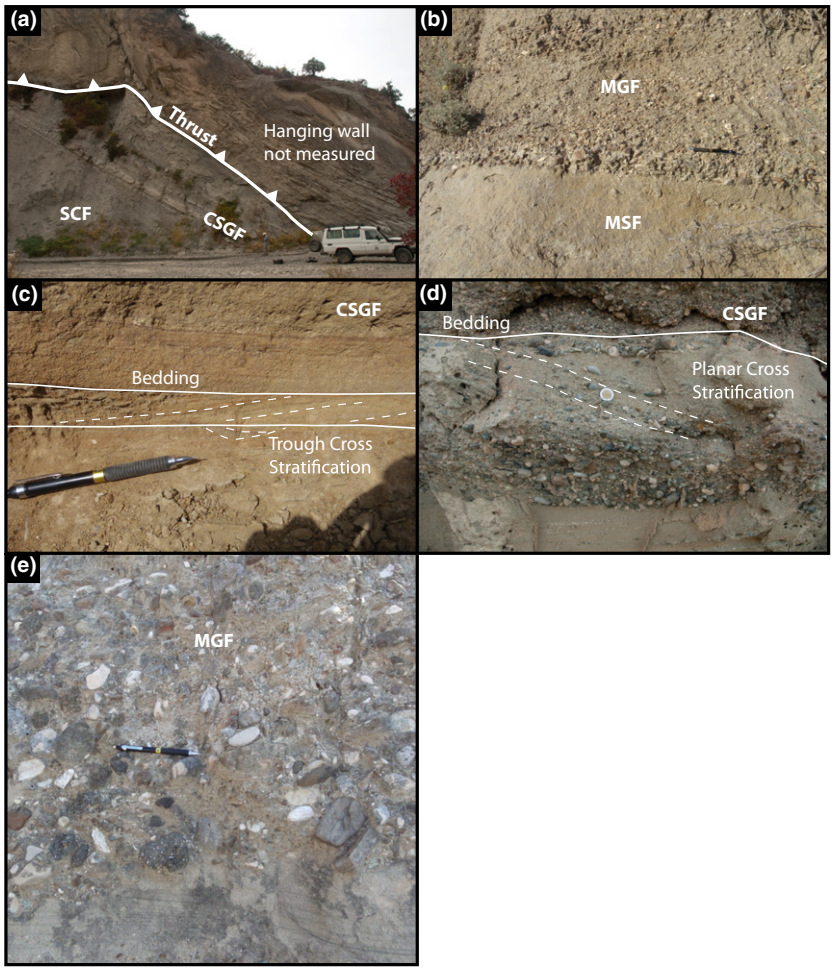

Fig. 3. Field photos highlighting examples of the litho-facies used in this study. (a) View northwest at the top of the Vashlovani section at a large package of unlaminated silt and clay facies (SCF) with a several metre thick package of cross-stratified sand gravel facies (CSGF). The north-dipping thrust represents the end of this section. (b) Contact between massive gravel facies (MGF) and massive silt facies (MSF) in the Sarica section. Note the lack of any major sedimentary structures in either package except limited graded bedding at the base of the massive gravel facies. (c) and (d) are both examples of cross-stratified sand and gravel facies illustrating the variability within this facies. Both exhibit cross-stratification, but the sand dominated version of this facies contains abundant centimetre-scale structures as in (c), where as the coarser grained versions tend to have decimetre to metre scale cross beds as seen in (d). (e) Massive gravel facies near the base of the Sarica section.

Table 2. Location of measured sections

Section	Coordinates of base	Coordinates of top
Vashlovani	46.360°E, 41.214°N	46.365°E, 41.237°N
Sarica	46.951°E, 41.052°N	46.953°E, 41.081°N

Lithostratigraphy and facies

The lower 850 m of the Vashlovani section comprise the V1 stratigraphic unit and are dominated by interleaving of 10–50 m-thick intervals of unlaminated silt and clay facies with 5–10 m-thick packages of cross-stratified sand and gravel facies and massive silt facies (Fig. 5). Trough and planar cross-stratification are common in the cross-stratified sand and gravel facies and some horizons exhibit limited pebble- to cobble-sized mud-clast conglomerate. Individual cross-stratified sand and gravel facies intervals are generally laterally traceable over hundreds of metres, but vary in thickness and coarseness. Silt content generally increases up-section, with unlaminated silt and clay facies intervals dominated by mottled clayey-silt at the base of the section and silty clay facies towards the top. Pedogenic carbonate nodules are present within the unlaminated silt and clay facies between 480 and 640 m (Fig. 5). The top 100 m of the V1 unit is dominated by unlaminated silt and clay facies.

The relatively fine-grained V1 interval is overlain by unit V2, which consists of a 155-m-thick succession of imbricated, clast-supported cobble to boulder conglomerate classified as massive gravel facies (Fig. 6). With the exception of sparse lenticular sandy-clay horizons, unit V2 is completely composed of coarse conglomerate. Both the lower and upper contacts of this interval are covered along the line of section. The V2 horizon, however, can be traced in satellite imagery due to its distinctive dark

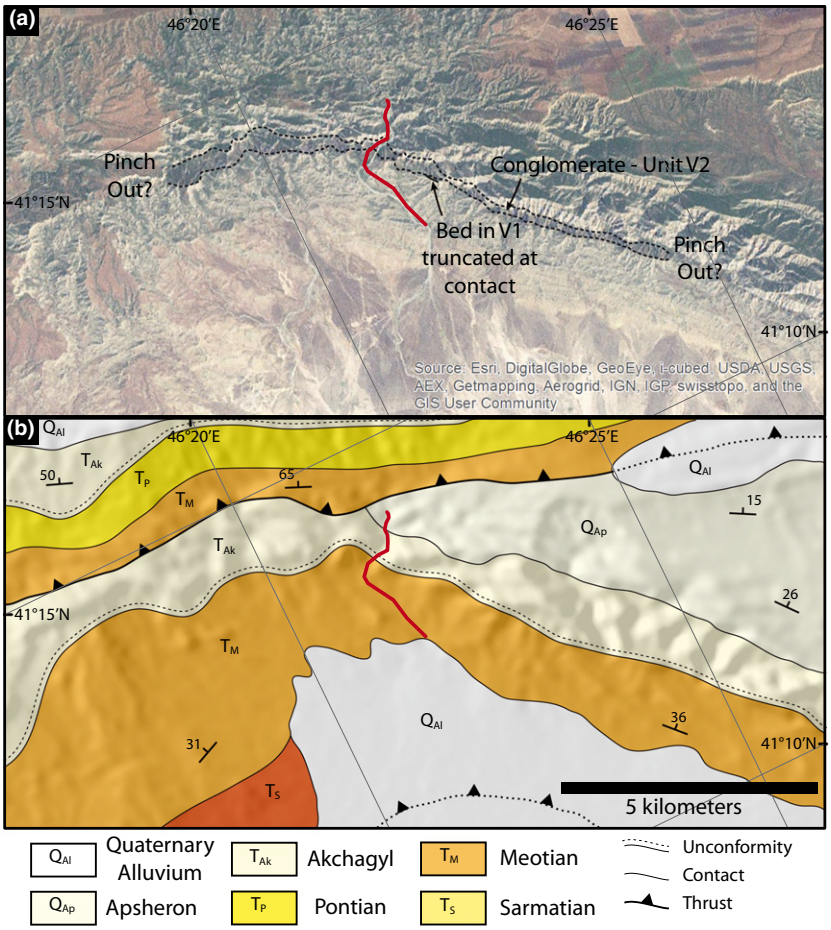

Fig. 4. Map of the Vashlovani study area. The dark red line in both images is the path along which the section was measured. (a) Satellite imagery with outlines of the conglomerate defining unit V2 outlined. Marker bed in the underlying unit V1 which is truncated into the contact between V1 and V2 is also highlighted, though it is important to note that this does not appear to be angular unconformity, rather that there is palaeo-topography on this contact. (b) Geologic map of the Vashlovani area from Abdullaev *et al*., (1957). Note that the contact between the Meotian and Akchagyl along the line of section is marked as an unconformity and roughly coincident with the location of unit V2 outlined in (a).

brown colour and tendency to form cliffs (Fig. 4a). In the satellite imagery, the V2 horizon appears to be relatively continuous over > 5 km, though the outcrop belt is in places obscured by landslides composed mostly of the overlying V3 unit. Additionally, in the imagery, continuous strata within V1 appear to truncate against the lower boundary of the V2 unit (Fig. 4a). The nature of the upper contact between V2 and V3 is more obscure, but we consider it conformable based on available evidence.

In the measured section the V3 unit overlies the coarse succession of unit V2 and comprises *ca*. 475 m of mixed unlaminated silt and clay facies, massive silt facies and cross-stratified sand and gravel facies. Within unit V3, the unlaminated silt and clay facies deposits are typically 15–30 m thick whereas the massive silt facies deposits range from 10 to 30 m thick and contain abundant intervals of cm-scale interlayers of clay and silt. The cross-stratified sand and gravel facies deposits in this upper succession are 5–10 m thick and are characterized by abundant fossil concentrations and planar cross-stratification. Plant material, including leaf impressions and remains of woody plants, are common within the upper portions of the finer-grained unlaminated silt and clay facies deposits. The top of the section is truncated by a north-dipping, south directed thrust fault (Fig. 3a).

Micropalaeontology

We collected and analysed four biostratigraphic samples from the Vashlovani section, including sample V-510 from unit V1 and samples V-1040, V-1260 and V-1465 from unit V3 (Figs 5, S1–S4; Appendix S2). Although unit V1 is characterized primarily by freshwater ostracods, mostly from the candonidae family, the assemblages do not constrain the age of this unit because these species are common in Paratethyan-related sediments from the Upper Miocene to present (Fig. S1). The three samples from unit V3 all indicate a change to brackish water conditions, being dominated by the foram *Ammonia beccarii* (Linné) and various different brackish water ostracod species (Figs S2–S4). The presence of *Ammonia beccarii* (Linné) suggests a salinity similar to the modern day

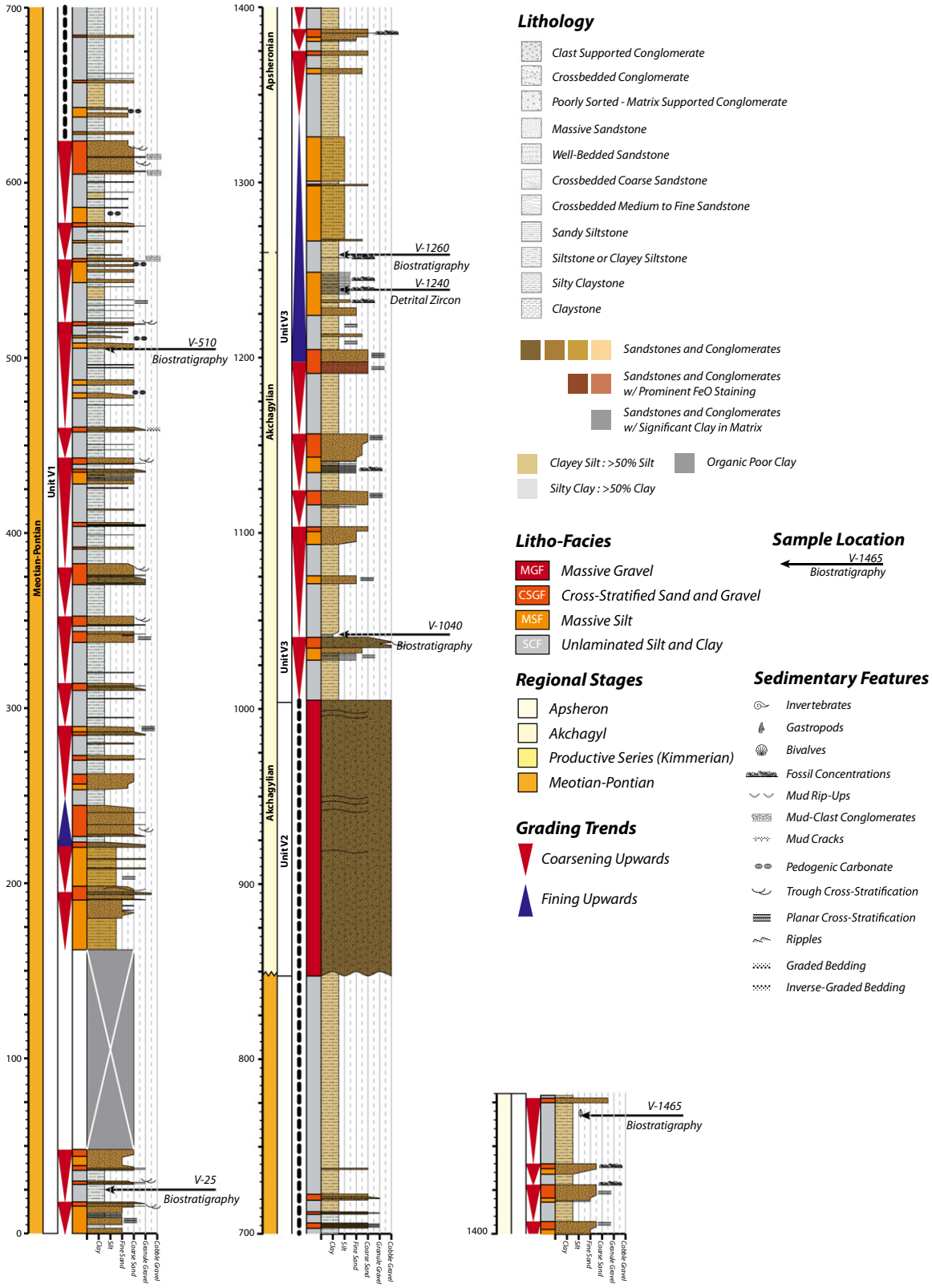

Fig. 5. Measured sections for the Vashlovani locality (see Fig. 1b for location and Fig. 4 for detailed geology). Section includes a simplified graphic column with grain size on the bottom axis and metres above base on the vertical axis. Lithologies are indicated with patterns and colours indicate relative colours in the field along with percentage of silt for finer-grained strata, see explanation to the right of the column. Estimates of regional stage boundaries within the measured section are based on previously published maps or studies. Boundaries for the Vashlovani section are from the Geological Map of Georgia (Gudjabidze, 2003), which are identical to an earlier 1 : 200 000 scale geologic map (Abdullaev *et al.*, 1957). Grading trends are indicated with blue and red triangles. See text for Discussion of assignment of facies.

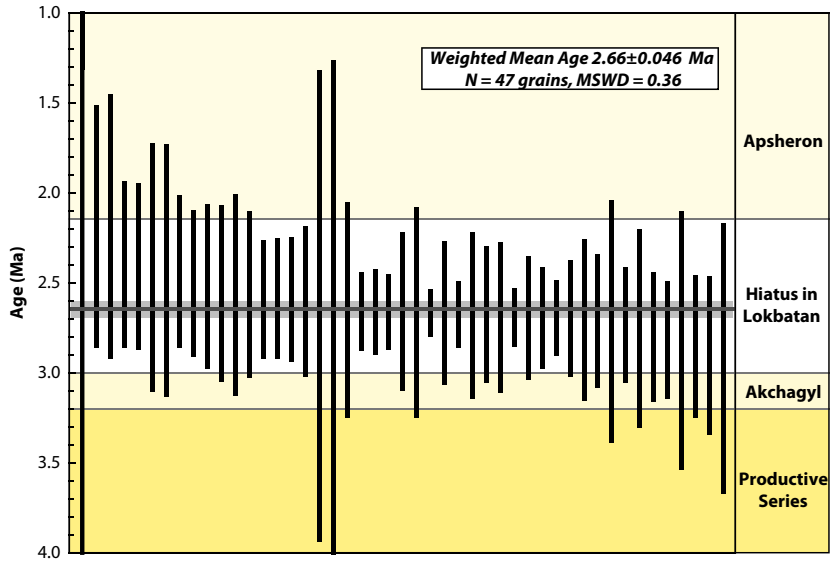

Fig. 6. Weighted average of 47 single-grain U-Pb zircons dates from sample V-1240, collected 1240 m above the base of the Vashlovani section. Error bars represent 2-sigma error, which was used to calculate the weighted average. The grey shaded zone represents the uncertainty on the weighted average. Ages of stage boundaries are from van Baak *et al.* (2013) as determined in the Lokbatan section on the Apsheron peninsular (Fig. 1) and are the same as in Figs. 2 and 10. Maximum depositional age for this sample corresponds to the depositional hiatus between the Akchagyl and Apsheron periods recognized by van Baak *et al.* (2013) on the Apsheron peninsula.

Black Sea, which is fresher than the open ocean, with a mean salinity of 17‰ in surface waters and up to 23‰ at depth (e.g. Boomer *et al.*, 2010). Assemblages similar to those found in unit V3 are most common in Apsheron-aged sediments of the Black and Caspian Seas, but the assemblages do not restrict the depositional age of this unit to the Apsheron because all of these fauna are present in older and younger sediments.

Interpreted depositional environments

Unit V1 is 850 m thick and records a predominantly fluvial environment with either meandering or anastomosing river networks. In this setting, unlaminated silt and clay facies represent flood plain deposition and the isolated massive silt facies likely record overbank deposits. The prevalence of soil carbonate concretions within the unlaminated silt and clay facies indicates that the floodplains were unoccupied long enough for soil to develop. These soil carbonates may further suggest a relatively arid environment. The cross-stratified sand and gravel facies deposits are interpreted as mainly channel deposits, consistent with the prevalence of trough cross-stratification. The lateral continuity of the cross-stratified sand and gravel facies deposits is consistent with deposition in meandering or anastomosing channels (e.g. Fielding *et al.*, 2012). The mud-clast conglomerate intervals likely record lateral erosion of fine-grained floodplain deposits.

Within the overlying unit V2, the absence of distinctive sedimentary features makes it difficult to infer details of the depositional environmental. However, the poor sorting of the conglomerates and lack of intervening sand suggests deposition in an alluvial fan or proximal distributary channel network (e.g. Nichols & Fisher, 2007; Fielding *et al.*, 2012). The nature of the lower and upper contacts of the V2 facies unit with the V1 and V3 units, respectively, were not well constrained in the field. Tracing of these contacts in Google Earth imagery and the truncation of beds in V1 against the lower contact of V2, suggests V2 is unconformable with respect to V1 (Fig. 4). The upper contact between V2 and V3 could also be unconformable based on the imagery, but this is less conclusive as this contact is often obscured by landslides formed from V3 material, thus we consider it conformable. The dramatically coarser average grain size in V2 suggests a more proximal source of sediment delivered across a steeper landscape, which if the pattern continued up-section could possibly reflect uplift of the watershed relative to the location of the measured section. However, the abrupt facies change represented by Unit V2 is likely more consistent with a temporary increase in sediment supply (e.g. Allen *et al.*, 2013; Ballato & Strecker, 2013).

The upper V3 unit contains primarily unlaminated silt and clay facies, massive silt facies, and cross-stratified sand and gravel facies deposits. This interval was likely deposited in a fluvial environment, which is supported by the presence of terrestrial fossils suggestive of sub-aerial deposition within unlaminated silt and clay facies in this interval. The generally thicker packages of cross-stratified sand and gravel facies deposits within unit V3 compared to unit V1 is most simply explained by an increase in sediment supply overtime (e.g. Blum & Törnqvist, 2000; Allen *et al.*, 2013). The cross-stratified sand and gravel facies strata within V3 are also predominantly finer grained and lacking the mud-clast conglomerate seen in the lower V1 unit, but still contain abundant shell

fragments. The lack of mud-clast conglomerates could indicate a lower carrying capacity during this time (i.e. less ability to erode and transport), which could be an indicator of higher accommodation space with less erosion of nearby flood plain deposits, or again consistent with increased sediment input. We favour the latter hypothesis, an increase in sediment input, as this is consistent with the general coarser nature of unit V3 with respect to V1. The abundant planar cross-stratification within the sand of V3 likely records lateral accretion and migration of channels in a broad flood plain, represented by the fine-grained material, within a meandering fluvial network (e.g. Fielding *et al.*, 2012).

U-Pb geochronology

The maximum depositional age of unit V3 is constrained by the youngest population of detrital zircons from sandstone collected 1240 m above the base, near the centre of unit V3 (Sample V-1240). The weighted mean average 206Pb/238U age from the 47 youngest grains (of 96 total zircons) yields a maximum depositional age of 2.66 ± 0.05 Ma (Fig. 6; Table S1). Additional results from detrital U-Pb ages of zircons from within the Kura Basin are discussed in detail by Forte (2012).

Sarica

The Sarica section is 2045 m thick and is located north of the Adjinour Playa in central Azerbaijan (Figs 1 and 7; Table 2). The section is located within the backlimb of the Sarica fold and was previously mapped as exposures of the Productive Series (Balakhany Suite), Akchagyl and Apsheron strata (Fig. 7, Ali-Zade, 2005). We divide the Sarica section into five stratigraphic units denoted S1–S5 (Fig. 8).

Lithostratigraphy

Interbeds of coarse sandstone and pebble to boulder conglomerate of the massive gravel facies characterize S1, which forms the basal 215 m of the Sarica section (Fig. 8). The succession is composed of a series of 15–25 m thick, fining upward intervals, starting with basal scours overlain by conglomerate, which grade upward into coarse to medium grained sand with isolated pebbles (e.g. Fig. 3d). Additionally, within unit S1 as a whole, conglomerate clast size decreases upwards, with cobble to boulder conglomerate near the base and pebble to cobble-conglomerate near the top of the succession. Although most conglomerate strata are clast-supported, some matrix-supported deposits are present (Fig. 9b). Planar cross-stratification is common in the coarse sand horizons, typically defined by strings of pebbles. Two palaeocurrent estimates within this interval suggest south-southwest flow (Fig. 8).

The S2 and S3 intervals consist of a 690-m-thick succession characterized by 50–100-m thick, coarsening-upward sequences composed of unlaminated silt and clay facies, massive silt facies, and cross-stratified sand and gravel facies. The basal 300 m of this succession defines unit S2 and contains 25–100 m thick intervals of grey clayey-silt that grade upwards to yellow-buff silty clay (both classified as unlaminated silt and clay facies) and are then capped by dark brown to red sand and conglomerate (classified as cross-stratified sand and gravel and isolated massive gravel facies). The sand in the S2 interval is generally coarse, occasionally trough cross-bedded, and

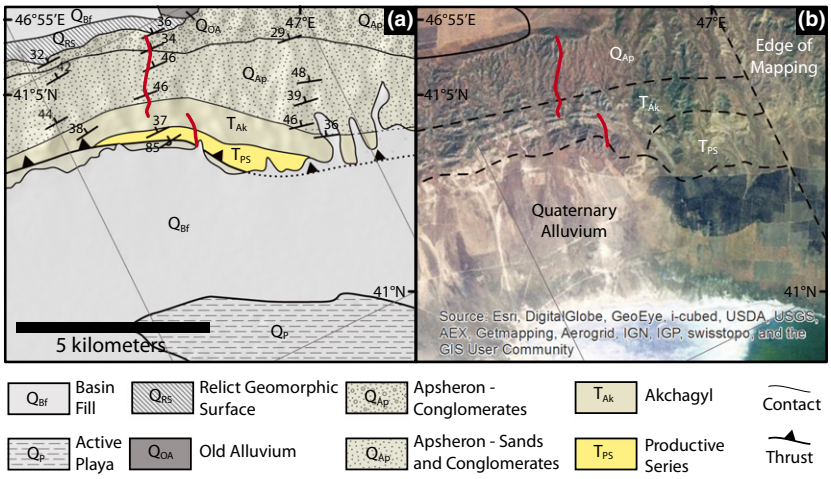

Fig. 7. Map of the Sarica study area. For both maps, the dark red line indicates the path of the measured section. The large jog in the section occurred in an attempt to follow a path with better exposure while maximizing the thickness of the section exposed. (a) New geologic map from our field work in 2008 for the Sarica region. The age assignments for units in this map are based on the correlations presented in this work. (b) Satellite imagery for the same region with an overlay of the mapping of Abdullaev *et al.*, (1957). Notice that the age of the units generally are consistent with our map shown in (a), but that the location of the Productive Series strata is incompatible with the clear stratal geometries visible in the imagery.

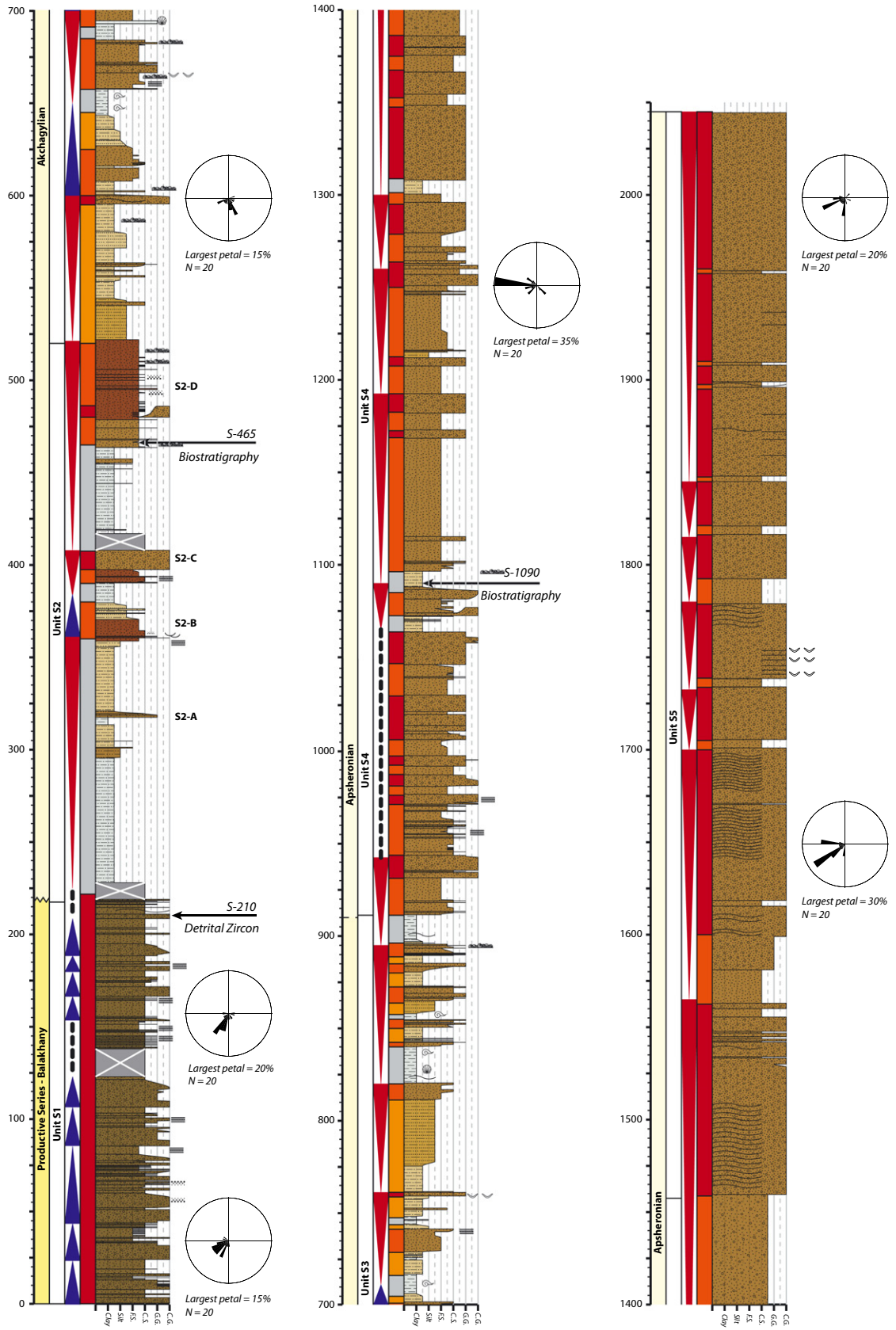

Fig. 8. Measured section for the Sarica locality, (see Fig. 1b for location and Fig. 7 for detailed geology). Approximate location of previously mapped stage boundaries are from the Geological Map of Azerbaijan (Ali-Zade, 2005). Rose diagrams indicate palaeocurrent estimates from measuring the long-axis of imbricated clasts, all other symbols the same as in Fig. 5. See text for discussion of assignment of facies. Note that the short break in section just above 400 m represents the point where the major jog in the measured section occurs visible in Fig. 7. This jog occurs along the top of the S2-C horizon marked in Fig. 9.

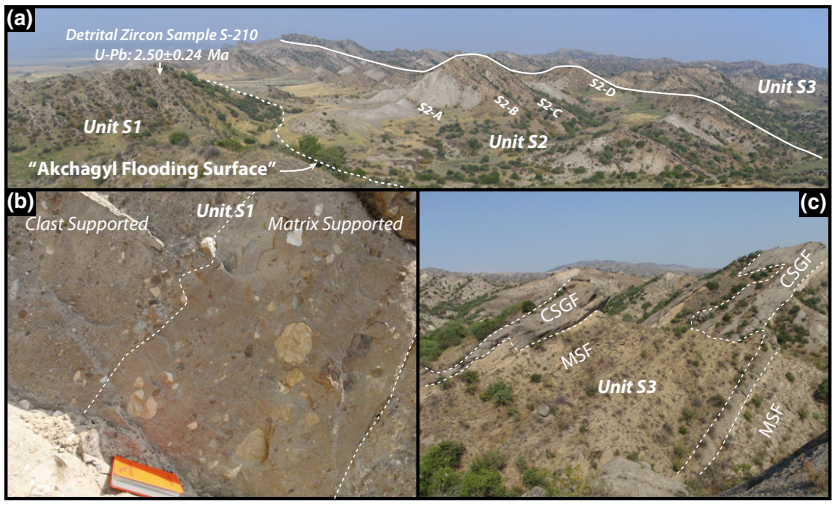

Fig. 9. Field photos from the Sarica measured section. (a) View west along the contact between the basal S1 and S2 units that represents the Akchagyl flooding surface in the interior of the Kura Basin. The horizons labelled S2-A, -B, -C and -D are laterally continuous within unit S2 over several kilometres and are labelled in the measured section (Fig. 8). Location of detrital zircon sample S-210 is shown along with maximum depositional age (Fig. 10). (b) Example of a matrix-supported interval within unit S1. (c) View northeast within unit S3 of preserved channel geometries within isolated bodies of cross-stratified sand and gravel facies.

contains abundant fossil concentrations and isolated coquina beds a few centimetres thick. In unit S3, between 525 and 910 m in the section, the thickness of the coarsening-upward sequences decreases, the percentage of unlaminated silt and clay facies drops significantly and deposits are instead dominated by massive silt facies and cross-stratified sand and gravel facies. The unlaminated silt and clay facies present are generally fossil rich with both gastropod and bivalve fauna. The sand within the cross-stratified sand and gravel facies is generally brownish grey and massive but contains abundant fossil concentrations and occasional small mud-clasts near the base. One palaeocurrent estimate ($N = 20$ measurements) within this interval indicates southeast-directed flow (Fig. 8).

The upper 1135-m-thick portion of the Sarica section is defined by units S4 and S5, which are generally much coarser sediment than the underlying strata. Unit S4 contains primarily cross-stratified sand and gravel facies and massive gravel facies with very rare horizons of massive silt facies. Both the sand and conglomerate in this interval contain few primary sedimentary structures, although this section is poorly exposed. Strata within S4 are generally coarse and laterally discontinuous, though the quality of exposure within the unit precludes detailed analysis of larger scale stratal geometries. Palaeocurrents within S4 conglomerate are dominated by west-directed flow (Fig. 8).

The upper 590 m of the section represent unit S5 and are almost exclusively massive gravel facies. Some internal coarsening-upward sequences are present, with coarse sand grading up to conglomerate. Conglomerate packages contain numerous internal scour planes, but the lithologies and grain sizes on either side of the scours are typically similar. Some scours are also associated with elongate, centimetre-scale mud clasts. Three palaeocurrent estimates within the S4–S5 interval show west-directed flow near the base that transitions to more southwest oriented flow up-section (Fig. 8).

Micropalaeontology

We do not have detailed micropalaeontology results from most of the Sarica section. Two samples collected from 465 m in Unit S2 and 1090 m in unit S4 generally contained highly fragmented shell materials or were otherwise poorly preserved. The sample from unit S2 did contain some examples of the foram *Ammonia beccarii* (Linné), which suggests a palaeosalinity similar to the modern day Black Sea.

Interpreted depositional environments

Unit S1, consisting of the basal 215 m of the section dominated by massive gravel facies, is interpreted as a braided fluvial system (e.g. Fielding *et al.*, 2012). The series of fining upward intervals within this unit likely represent migration of channels and bars within a braid plain. The conglomeratic deposits have scours at their bases, suggesting erosion into pre-existing bars with avulsion and channel migration leading to the deposition of the medium to coarse sand as a new bar is established. The relatively consistent south- to southwest-directed palaeocurrent data from both the top and bottom of the unit are consistent with a south flowing series of braided channels. Isolated matrix supported, poorly sorted conglomerate suggest occasional deposition from debris flows, indicating that the braid plain was relatively proximal to a steep slope. This suggests unit S1 was sourced from the Greater Caucasus Mountains and is consistent with a high sediment yield during a period of relatively low base level (e.g. Blum & Törnqvist, 2000; Allen *et al.*, 2013).

The boundary between unit S1 and S2 records a dramatic change to a more distal depositional environment, e.g. a marginal lacustrine to fluvial environment, represented by the silt and clay facies (Figs 8 and 9a). The presence of forams indicates that the fine-grained unlaminated silt and clay facies deposits record periods of sub-aqueous deposition in a semi-saline environment, requiring a standing body of water potentially connected to the Caspian Sea. The sand and conglomeratic horizons may record either sub-aqueous deposition at the lake margin as Gilbert-delta deposits, or in a meandering or braided fluvial setting. However, the lateral continuity of cross-stratified sand and gravel strata suggests periods of relative stability in base level, generation of accommodation space and sediment supply (e.g. Blum & Törnqvist, 2000). We hypothesize that small, coarse grained Gilbert deltas are the most likely depositional environment for this succession given the presence of forams.

The decrease in the abundance of unlaminated silt and clay facies in the overlying unit S3 suggests that this interval records a more proximal meandering or anastomosing fluvial network than S2, suggesting progradation between S2 and S3. The presence of mud rip-up clasts and shell concentration suggest erosion of surrounding finer-grained intervals, consistent with a fluvial environment. Additionally, both in the field and in satellite imagery, individual cross-stratified sand and gravel facies packages are not laterally continuous, with some preserving channel morphologies (Fig. 9c). The massive silt facies are interpreted to represent overbank and floodplain deposits with the unlaminated silt and clay facies likely indicating deposition in a more distal portion of the floodplain. The unlaminated silt and clay facies in this interval are very fine grained but lack clear laminations. They are rich in bivalve and gastropod shells, which is consistent with floodplain deposits but may also indicate periodic inundation by a shallow lake.

Taken together, the succession of environments we interpret for units S1, S2 and S3 may represent flooding of a relatively high sediment yield fluvial system by base-level rise followed by deltaic deposition. In this scenario, the basal S1 unit represents either a fluvial or distal alluvial fan and the S1–S2 transition suggests a sudden rise in base level. A supply of coarse sediment is still available leading to accumulation of Gilbert-type deltas during the deposition of S2.

Unit S4 records a renewed influx of coarse sediment relative to unit S3 (Fig. 8), and likely represents an anastomosing or braided fluvial network. The significance of the west-directed palaeocurrent measurement in S4 is unclear. On the basis of the dominance of poorly sorted coarse conglomerate in unit S5, we interpret this unit as representing deposition in an alluvial fan or proximal distributary fluvial network (e.g. Fielding *et al.*, 2012). The upward coarsening suggests progradation of the fan complex. In general, the transition from deltaic deposition in unit S3 to the coarse clastic, alluvial fan deposition in S5 requires uplift of the watershed and a proximal source for the conglomerate, perhaps related to propagation of structural systems southward into the Kura Basin and Kura fold-thrust belt (e.g. Forte *et al.*, 2013).

U-Pb geochronology

The maximum depositional age of the base of this succession is constrained by the youngest population of detrital zircons from sandstone collected 210 m above the base, near the top of unit S1 (Sample S-210). The weighted mean average of four 206Pb/238U ages from the three youngest grains (one grain was sufficiently large to analyse twice) yields a maximum depositional age of 2.5 ± 0.2 Ma (Fig. 10; Table S1). The three zircons analysed are part of a population of 100 detrital U-Pb ages of zircons discussed in detail by Forte (2012).

DISCUSSION

Correlations to regional stages and Caspian base level

To correlate the Vashlovani and Sarica sections to each other and the regional time scale, we use a sequence stratigraphic approach (e.g. van Hinte, 1978; Steenwinkel, 1990; Van Wagoner & Bertram, 1995) and rely primarily on apparent changes in base level interpreted from changes in depositional environments within each section. It is important to note that our estimates of relative changes in base level are based on a balance between accommodation space relative to sediment supply resulting in the changes in depositional environment. We do not have independent evidence of actual water depth within these sections (e.g. Immenhauser, 2009), thus these are inferred changes in base level. These inferred

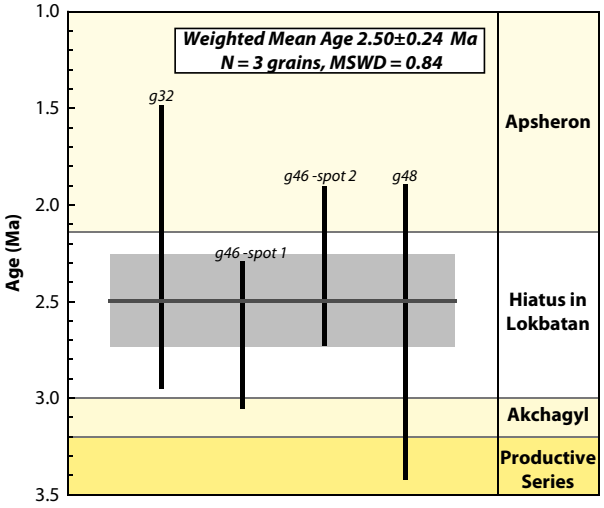

Fig. 10. Weighted average of 4 U-Pb dates from three detrital zircon grains from sample S-210, collected 210 m above the base of the Sarica section. All symbols are the same as in Fig. 4. Maximum depositional age for this sample corresponds to the depositional hiatus between the Akchagyl and Apsheron periods recognized by van Baak *et al.* (2013) on the Apsheron peninsula.

base-level changes are then used to correlate the sections to each other and then ultimately to variations in Caspian base level and the regional time scale (Forte & Cowgill, 2013). Additional constraint for the presented correlations also comes from previous mapping efforts (Abdullaev *et al*., 1957; Nalivkin, 1976; Gudjabidze, 2003; Ali-Zade, 2005). Although our correlation methodology is largely similar to a traditional sequence stratigraphic approach and the Caspian regional stages generally can be characterized in a sequence stratigraphic framework, we do not formally define sequences and systems tracts. Where possible, we do use additional temporal constraints from the available micropalaeontology and U-Pb geochronology of detrital zircons as described above.

The Sarica and Vashlovani sections have previously been interpreted as representing the late Miocene through Pleistocene, with Vashlovani exposing the Meotian-Pontian through Apsheron (Fig. 4) and Sarica exposing Productive Series through Apsheron-aged strata (Fig. 7, Gudjabidze, 2003; Ali-Zade, 2005). Our proposed correlations do not substantially differ from these previous assignments. In the Sarica section, we correlate the basal conglomeratic unit, S1, to the Productive Series, and the abrupt up-section change to finer-grained sediment within unit S2 as representing the large transgression at the Productive-Akchagyl stage boundary (Fig. 11). We favour this correlation because it is both easily explained with changes in relative base level predicted by the Caspian base level curve and largely consistent with recent published mapping of this area (e.g. Ali-Zade, 2005) and our own mapping (Fig. 7). The transition in depositional environments inferred for units S2 and S3 suggests a fall in base level, and may suggest S3 is largely correlative to the lower Apsheron. Units S4 and S5 generally record a progressive coarsening, which could be interpreted either in terms of a steady base-level fall or tectonic uplift of the watershed and increase in sediment supply. We favour a tectonic explanation because a large-scale and long-term coarsening-upward succession generally does not correspond to the Caspian base level record. This coarsening-upward trend precludes any detailed correlation between these upper packages and the regional stages, because of the relatively monotonous nature of units S4 and S5, the absence of clear signatures of changes in base level, and the absence of any material allowing absolute dating, such as ash horizons.

The above correlation scheme for the Sarica section is consistent with more recent work (2005), but is somewhat at odds with older work from 1957 to 1976. In particular, the 1 : 500 000 scale geologic map of Azerbaijan (Ali-Zade, 2005) shows the base of Sarica as exposures of the Productive Series, specifically the Balakhany suite. Contrastingly, both the older 1 : 1 000 000 scale regional map (Nalivkin, 1976) and a 1 : 200 000 scale geologic map (Abdullaev *et al*., 1957) show the measured exposures of unit S1 as Akchagyl in age. However, these maps do illustrate an exposure of the Productive Series due east of the location of the measured section, within strata that are correlative with the overlying S2 unit on the basis of field evidence and satellite imagery (Fig. 7b). Additionally, the lithologic description of the Productive Series sediments for the 1 : 200 000 scale map is the most consistent with the observations of unit S1. Thus, we hypothesize that this discrepancy may be due to errors in the location of contacts on the older map series. Our new field mapping of the area surrounding the Sarica section clarifies the location of the Productive Series rocks (Fig. 7a) and is generally consistent with recent geologic map of Azerbaijan (Ali-Zade, 2005), though is more detailed in terms of structures, geomorphic and neotectonic features and lithologic differences within the Apsheron strata.

The Productive Series is typically presumed to extend from *ca*. 5.6 to 3.2 Ma (Fig. 2). Thus, it is essential to note that correlation of unit S1 to the Productive Series appears to conflict with the maximum depositional age of 2.5 $\pm$ 0.2 Ma reported above from the youngest population of detrital zircons found in a sample from this unit (Fig. 10). The most reasonable explanations for this discrepancy are that (1) the Akchagyl transgression was younger at the more distal location of the Sarica section in the interior of the Kura Basin than at the Caspian coast, as expected for a diachronous flooding surface, (2) the correlation is wrong and unit S1 is not correlative to the Productive Series or (3) the constraint on the depositional age of S1 from the detrital zircons is erroneous. The follow section explores these scenarios in more detail and concludes that the first explanation is the most likely because it is consistent with pre-existing data and the population of detrital zircons meets all the criteria for a statistically significant maximum depositional age.

The Vashlovani section seems to record only first-order changes in base level. We correlate the basal, fluvially dominated unit V1 to the Meotian and Pontian regional stages, conglomeratic unit V2 to the Productive Series, and fluvial unit V3 to the Akchagyl and Apsheron (Fig. 11). This is largely consistent with previous maps, except the prior work shows an unconformity between the Meotian-Pontian stage and the Akchagyl, with the Productive Series missing (Fig. 4b, Abdullaev *et al*., 1957; Gudjabidze, 2003). Previous descriptions suggest that the Akchagyl locally contains a basal conglomerate horizon, but they do not discuss the thickness of this conglomerate (e.g. Azizbekov, 1972; Isaneva & Sadngova, 1999). However, the total thickness of the Akchagyl in this region has been described as not exceeding *ca*. 200 m (e.g. Azizbekov, 1972), which would suggest that the *ca*. 150 m conglomeratic V2 horizon is too large to be a portion of the Akchagyl as previously described. In addition, based on satellite imagery, unit V2 is unconformable with respect to the underlying strata and while continuous within the *ca*. 5 km area surrounding the measured section, this horizon does not appear to continue much beyond this region (Fig. 4a). Although this deposit could reflect a palaeo-Kura river (e.g. Isaneva & Sadngova, 1999), we instead favour the interpretation that the conglomeratic V2 horizon represents the whole Productive

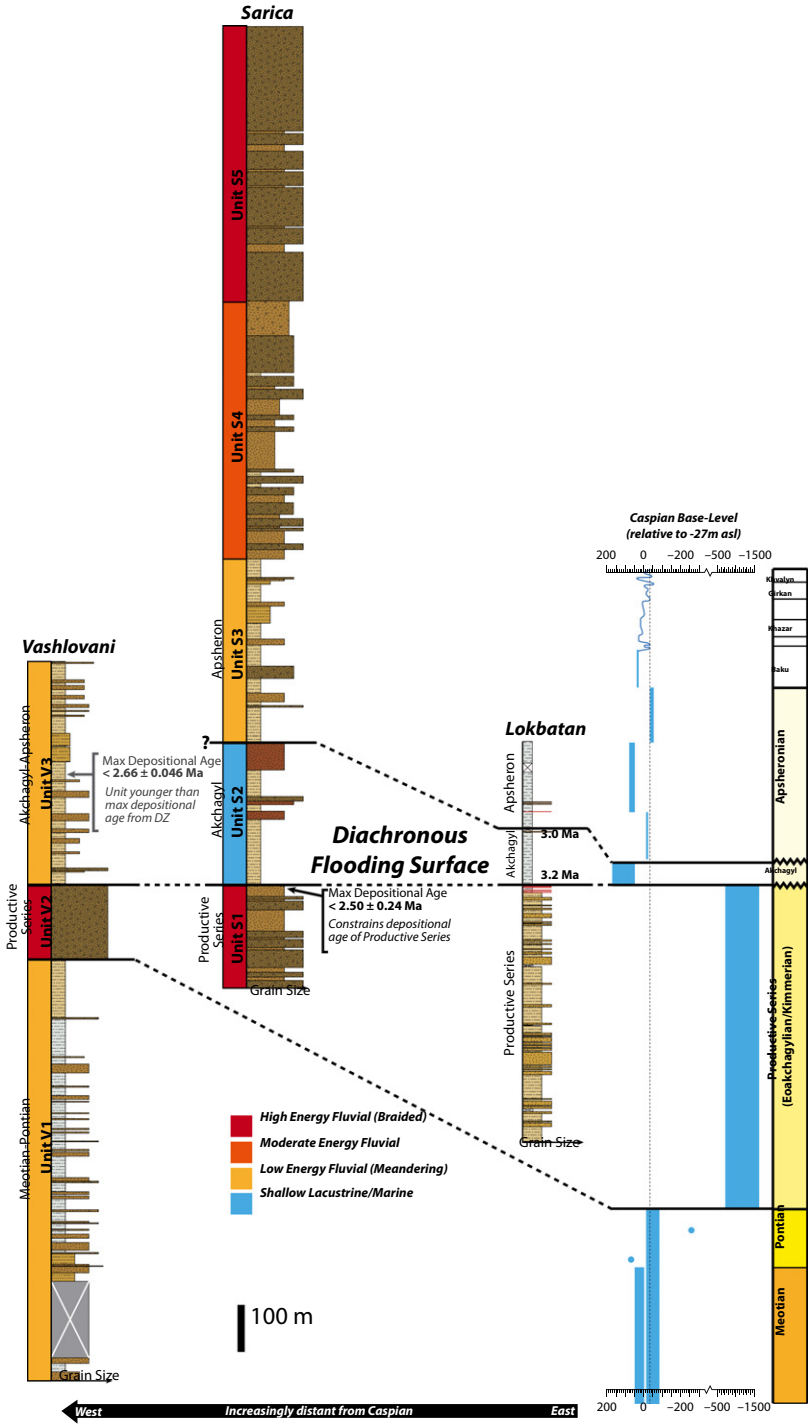

Fig. 11. Correlations between the Sarica and Vashlovani measured sections and Caspian regional timescale based primarily on variations in base level inferred from depositional facies. Caspian base level curve used for correlation is modified from Forte & Cowgill (2013). Maximum depositional ages from the two samples described in the text are shown in their stratigraphic location. Maximum depositional age for Unit S1 is assumed to be close to the true depositional age of the unit because this maximum depositional age is younger than the presumed age of the Productive Series. Maximum depositional age for Unit V3 is not useful for constraining the true depositional age of the unit, and thus not useful for correlation, because the presumed age is younger than that determined from the detrital zircons. The correlation between the Akchagyl-Apsheron boundary in the Sarica and Vashlovani sections is unclear, represented by the '?' to the left of this boundary in Sarica. Lokbatan stratigraphic section is a simplified relative to the original presented by van Baak *et al.* (2013). Correlations between the Lokbatan section and regional stages are taken directly from van Baak *et al.* (2013). See text for discussion of correlation scheme for Vashlovani and Sarica.

Series, representing a period of increased sediment yield and primarily deposition of coarse material during a lowstand in Caspian base level, consistent with previous models of expected responses to low base levels (e.g. Shanley & McCabe, 1994; Blum & Törnqvist, 2000). This unit may thus represent a broad distributary fluvial network

that existed at this time (e.g. Nichols & Hirst, 1998; Nichols & Fisher, 2007; Fielding *et al.*, 2012). Pairing this interpretation with preliminary results of provenance work from a sample within unit V2, which suggests a source of sediment virtually devoid of lithic clasts (Forte, 2012), portrays an environment with extensive local reworking of sediment. This local reworking suggests minimal generation of accommodation space and thus relatively low basin subsidence.

In the overlying V3 unit, there are no significant lithologic changes to suggest a transition from the Akchagyl to the Apsheron (Fig. 11). Although, previous maps (Abdullaev *et al.*, 1957; Gudjabidze, 2003) place this boundary roughly coincident with the dated detrital zircon sample from the Vashlovani section (Fig. 5), the map resolution is such that the sample is equally likely to come from Akchagyl- or Apsheron-aged sediments. If the sample is from Akchagyl-aged deposits, which are dated *ca*. 3.2 to 3.0 Ma in the Lokbatan section (Fig. 2), then the maximum depositional age of 2.66 ± 0.05 Ma reported above would be anomalously young relative to the South Caspian chronostratigraphic timescale similar to the case for unit S1 above. However, if the detrital zircon sample is from Apsheron-aged deposits, which are dated to *ca*. 2.1 to *ca*. 0.9 Ma (Fig. 2), then it does not require a change to the time scale, considering that the detrital zircon age provides only a maximum age for the timing of deposition. Because of the ambiguity regarding the location of the Akchagyl-Apsheron stage boundary within unit V3 in the Vashlovani section, we have elected to not choose between these competing scenarios. The relative increase in coarse sediment between V1 and V3, which we interpret as a potential increase in sediment supply, is most simply explained within the context of initiation of rapid uplift of the Greater Caucasus that began at *ca*. 5 Ma (e.g. Avdeev & Niemi, 2011).

Implications for the diachroneity of the Productive Series – Akchagyl Stage Boundary

The preferred correlation between the stratigraphy of the northern Kura Basin and the Caspian base level curve (Fig. 11) implies that the Akchagyl transgression was diachronous and occurred later in the interior of the Kura Basin than on the margin of the Caspian, *ca*. 250 km to the east. Within the Sarica section, the previous mapping, new U-Pb ages of detrital zircons, and the interpreted depositional environments are not consistent with the ages of the Caspian regional stage boundaries determined in the Lokbatan section. Both previous mapping (Abdullaev *et al.*, 1957; Nalivkin, 1976; Ali-Zade, 2005) and our preferred sequence stratigraphic correlation (Fig. 11) assign unit S1 in the Sarica section to the Productive Series. However, the zircon ages from near the top of the basal S1 unit indicate a maximum depositional age of 2.5 ± 0.2 Ma (Fig. 10), which is too young for the *ca*. 5.6 to 3.2 Ma age of the Productive Series stage as determined at Lokbatan, near the Caspian Sea coast (Figs 2 and 11, van Baak *et al.*, 2013). According to the dates of regional stage boundaries from Lokbatan, an age of 2.5 ± 0.2 Ma should correspond to a depositional hiatus between the Akchagyl and Apsheron stages, however this hiatus is likely a local effect related to initiation of deformation in this region (Fig. 2, van Baak *et al.*, 2013). Even at the maximum limit of the uncertainty in the U-Pb age (i.e. 2.7 Ma), the sample from S1 is still too young to have been deposited during the Productive Series as described at Lokbatan (van Baak *et al.*, 2013). It is important to note that such discrepancies are only exacerbated, if the true depositional age of the dated sample in S1 is actually younger than the maximum depositional age of 2.5 ± 0.2 Ma.

The anomalously young maximum depositional age of unit S1 is easily reconciled with the ages of stage boundaries at Lokbatan if the boundary between the Productive Series and Akchagyl stages is at least 0.5 Myr younger in the interior of the Kura Basin than in the Lokbatan section to the east. In this case, the transgression that defines the boundary between the Productive Series and Akchagyl stages reached the interior of the Kura subbasin later than in the Caspian Basin proper. Differences between the ages of stage boundaries at Lokbatan and those from the interior of the Kura Basin are not unexpected. The Lokbatan section is *ca*. 250 km east of the Sarica section. During the deposition of much of the Productive Series, Lokbatan was located on the palaeo-Volga Delta, likely on a broad ramp similar to the modern Volga Delta (e.g. Reynolds *et al.*, 1998; Vincent *et al.*, 2010). In addition, Lokbatan is now *ca*. 250 m below the topographical base of the Sarica section. The relative palaeo-elevations of these two sites are not constrained, but given the relatively high sedimentation rates recorded in Lokbatan during accumulation of the Productive Series (e.g. van Baak, 2010), we hypothesize that subsidence rates at Lokbatan were higher than at Sarica and thus possibly an even larger elevation differential existed between the two locations (Fig. 12a).

Based on the maximum depositional age of unit S1 from the detrital zircons, coarse sediment continued to accumulate at Sarica during the transition from the upper Productive Series (Surakhany Suite) to the Akchagyl Stage that occurred at *ca*. 3.2 Ma in Lokbatan (van Baak *et al.*, 2013). These age relationships suggest that Caspian waters did not reach the interior of the Kura Basin until at least after *ca*. 2.7 Ma (using the lower boundary of the error associated with the U-Pb detrital zircon age) due to the difference in palaeo-elevation between the two locations (Fig. 12). This interpretation is consistent with more general results that indicate basin topography can cause transgressions to appear later in the interior, higher elevation portions of subbasins (e.g. Catuneanu *et al.*, 1998; Liu *et al.*, 1998). We have no constraint for what subdivision of the Productive Series (typically referred to as 'suites') is represented by the coarse grained material at the base of the Sarica section, though previous mapping

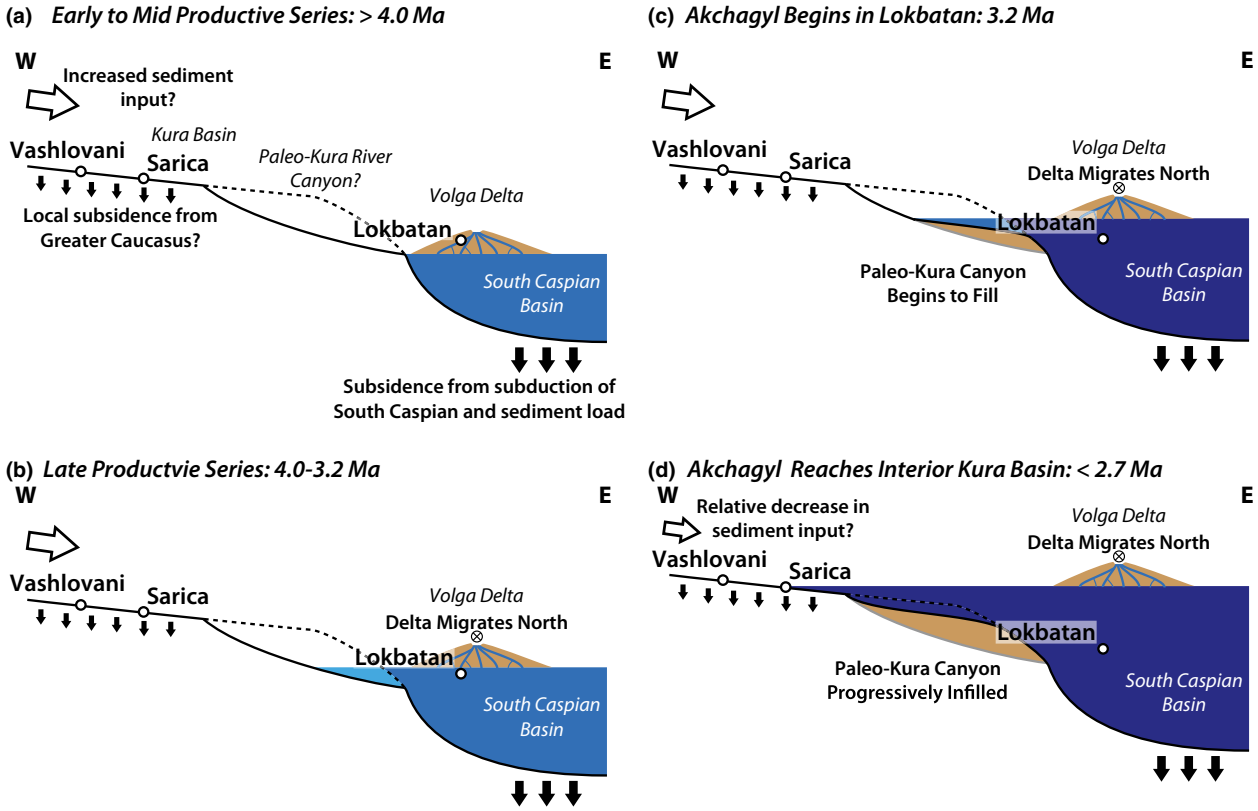

Fig. 12. Schematic cross section through the Kura and South Caspian Basins during transition from Productive Series to Akchagyl. (a) During the deposition of the Productive Series, base level was generally low and restricted to the deep part of the South Caspian basin. The Lokbatan section, from which the constraint for the regional time scale is derived, was deposited in the Volga Delta at a palaeo-elevation likely significantly below the Sarica section. Deposition in the interior of the Kura Basin was likely facilitated by local subsidence related to the growth of the Greater Caucasus. (b) During the latter half of the Productive Series (Sabunchi and Surakhani Suites) base level within the Caspian began to slowly rise and Lokbatan was submerged (projection of delta beneath water not shown). As Caspian base level rose and the Volga delta migrated north (as indicated by the circled x). (c) The Akchagyl transgression began in the South Caspian Basin at *ca*. 3.2 Ma and was marked by a rise in base level and a potential connection to the global ocean or Mediterranean, indicated by a change to darker blue water in the cartoon, which contributed to the distinctive microfauna which defines the stage biostratigraphically (e.g. Zubakov, 2001; Popov *et al.*, 2006). The rise in base level also began the process of filling in the canyon carved into the Kura Basin during the Productive Series (e.g. Kroonenberg *et al.*, 2005). (d) As the Akchagyl transgression continued, Caspian base level eventually increased sufficiently to reach the Sarica section and end deposition of the facies which define the Productive Series in this location sometime after *ca*. 2.7 Ma (based on the lower bound of the maximum depositional age).

indicates that these conglomerates are part of the Balakhany Suite (Ali-Zade, 2005). It is possible that the basal conglomeratic package represented by S1 in Sarica is similar to the V2 unit in Vashlovani, namely an interval representing the whole of the Productive Series deposition in the northern Kura Basin, however this interpretation remains speculative because the base of the Productive Series is not exposed in the Sarica area.

It is important to note that these results suggesting a diachronous Akchagyl flooding event are inconsistent with previous dating of the Kvabebi stratigraphic section further to the west in Georgia (Fig. 1, e.g. Agustí *et al.*, 2009). The Kvabebi section is a *ca*. 170 m long siliciclastic, coarsening-upward section also located within the Kura fold-thrust belt, in a generally similar position within the Kura basin (e.g. distance from the modern Greater Caucasus rangefront) as Sarica and Vashlovani. The base of the Kvabebi section is characterized by a distinctive dark blue clay horizon that contains mollusks and ostracods associated with the Akchagyl regional stage (Agustí *et al.*, 2009). The main goal of the study presented by Agustí *et al.* (2009) was to date a mammalian faunal site within this finer-grained interval and as such, the authors do not extensively discuss the correlations to the regional Caspian stratigraphy. Agustí *et al.* (2009) use a combination of magnetostratigraphy and Eurasian mammalian biostratigraphy to date the lower, *ca*. 100 m thick, fine-grained portion of this section that contains the reported Akchagylian fauna, and find that it spans between *ca*. 3.3–2.7 Ma (Agustí *et al.*, 2009). Though based on the data presented by Agustí *et al.* (2009) the base of the Akchagyl is not exposed, these dates, however, are more consistent with the age of the Productive Series – Akchagyl stage boundary as determined in the Lokbatan section. This is problematic because our model would predict that sections further to the west and in the same

general basin location (e.g. Kvabebi) would exhibit a similar diachroneity in the Productive Series – Akchagyl boundary as documented in Sarica.

Although our preferred interpretation is that the Akchagyl flooding surface is diachronous, as noted above, two alternative explanations for the anomalously young depositional age for unit S1 at Sarica can be posited. The first is that correlations of S1 to the Productive Series and S2 to the Akchagyl are incorrect. This is a tenable alternative, especially given that we do not have detailed biostratigraphic results for the Sarica section and the apparent inconsistency with the Kvabebi results. A rapid local increase in subsidence, local damming of rivers by growth of folds to the south of the Sarica area, or a sudden decrease in the availability and/or transport of coarse sediment could cause an apparent base-level rise, leading to the abrupt transition between the conglomerate and coarse sands of unit S1 and the clays and silts at the base of S2. However, there is no clear evidence for any of these processes and thus a large increase in Caspian base level associated with the Akchagyl transgression remains the simplest explanation for these particular observations at present.

Another possibility is that units S1 and S2 do correlate to the Productive Series and Akchagyl, respectively, but that the maximum depositional age constrained from the U-Pb ages of detrital zircons from sample S-210 is erroneous. The use of detrital zircon U-Pb geochronology to constrain maximum depositional age can be problematic, however, problems with this method mostly relate to the probability that the youngest grains will not be present in a given sample (e.g. Andersen, 2005). This is not of particular concern in this case, because even if a significant population of zircon grains younger than 2.5 $\pm$ 0.2 Ma was missed, the implication would be the same and instead imply an even larger diachroneity in the Productive Series – Akchagyl stage boundary. An additional relevant concern with detrital zircon geochronologic datasets is the statistical significance of a particular group of ages (e.g. Vermeesch, 2004; Andersen, 2005; Gehrels, 2012). Although there is some disagreement on the number of dated grains required to accurately constrain all of the age populations within a detrital zircon population, 100 grains, the number analysed in sample S-210 (Forte, 2012), is typically considered the standard for a robust, initial analysis (e.g. Gehrels, 2012). With a total population size of 100 grains, the three youngest grains from S-210 do define a statistically significant age population and there are no apparent reasons to exclude these analyses based on standard data filtering procedures (e.g. Gehrels *et al.*, 2008). In addition, the presence of these particular aged young zircons is not surprising, given that the youngest age population from S-210 overlaps in error with the extremely large (defined by 47 of 96 grains) youngest age peak of 2.66 $\pm$ 0.05 Ma in sample V-1240 (Fig. 6), indicating that there was a source terrain contributing sediment to the northern Kura Basin containing zircons with ages between 2.7 and 2.5 Ma.

If our preferred correlations of the lower parts of the Sarica section and maximum depositional age for unit S1 are correct, then it follows that the Akchagyl transgression was much more diachronous than previously suggested, at least as recorded in the area near Sarica. This result implies that the absolute ages of units mapped as Productive Series or Akchagyl in the interior Kura Basin have the potential to be in the order of 0.5 Myr younger than units similarly mapped near the Caspian Sea, which has important implications for the structural history of the Kura fold-thrust belt, considering that unconformities have been used to bracket the initiation age of structures (e.g. Forte *et al.*, 2010), which we discuss in the following section.

Using 3.2 and 2.7 Ma as the beginning of the Akchagyl in the Lokbatan and Sarica sections, respectively, and the current elevations of the bases of these sections implies a *ca.* 0.5 mm yr^{-1} rate of base-level rise, in the orders of magnitude smaller than the *ca.* 10 cm yr^{-1} rate of Caspian Sea level change observed during the Holocene (e.g. Karpytchiev, 1993; Kroonenberg *et al.*, 1997; Rychagov, 1997; Sedletskii & Baikov, 1997; Li *et al.*, 2004; Kozhevnikova & Shveikina, 2008; Rumyantsev *et al.*, 2008). This is also an overestimation of the rate of base-level change because the Lokbatan section was already inundated prior to the initiation of the Akchagyl stage (Fig. 12, van Baak *et al.*, 2013). However, in addition to the poorly constrained palaeo-elevations of these two locations, it is important to consider that by the time the interior of the Kura Basin was flooded with Caspian waters during the Akchagyl, very large increases in the total volume of the Caspian Sea would have been required to continue base-level rise, due to the large areal extent of the Caspian Sea during the peak of the Akchagyl stage (Fig. 1a).

Although the current lack of palaeo-elevations for the Sarica and Lokbatan sites make the previous analysis of base-level rise rate likely erroneous, we are able to estimate a rate of shoreline advance with slightly more confidence. Regional and local investigations of the tectonics of the eastern Greater Caucasus and Kura fold-thrust belt show no clear evidence of significant strike-slip structures capable of translating Sarica or Lokbatan in an east-west direction (e.g. Jackson *et al.*, 2002; Allen *et al.*, 2003; Forte *et al.*, 2010), thus the distance currently between the two sites has likely not changed significantly. Again using 3.2 and 2.7 Ma as the initiation of the Akchagyl stage in Lokbatan and Sarica, respectively, and an approximate distance of 250 km between the two sites, yields a rate of *ca.* 5 m yr^{-1}. This estimate is again, however, is likely an overestimate because the Lokbatan section was already inundated at the beginning of the Akchagyl.

At present, there is also not abundant evidence for a shift in the location of the depocentre from the South Caspian to the Kura basin during the Akchagyl transgression, as has been observed in other sub- and main basin pairs (e.g. Munteanu *et al.*, 2012). As noted earlier, there is a depositional hiatus observed between the Akchagyl and Apsheron stages in the Lokbatan section, which

would be consistent with a shift in depocentre location, but coincidence of this hiatus with an angular unconformity in the field points to a structural, rather than stratigraphic, explanation (van Baak *et al.*, 2013). However, it remains possible depocentre migration and sediment starvation in the South Caspian during the latter half of the Akchagyl stage may have, at least in part, contributed to this hiatus, but this remains speculative.

Finally, these results serve to further highlight potential problems stemming from inconsistent definition of the Akchagyl in either sequence or biostratigraphic terms, which is more thoroughly discussed by van Baak *et al.* (2013) and Forte & Cowgill (2013). For the Sarica section, we have defined the Akchagyl in a sequence stratigraphic sense, consistent with prior work (e.g. Abreu & Nummedal, 2007; Green *et al.*, 2009), whereas in the Lokbatan and Kvabebi sections, the Akchagyl is defined biostratigraphically (Agustí *et al.*, 2009; van Baak *et al.*, 2013), also consistent with prior work (e.g. Zubakov, 1992; Jones & Simmons, 1996). The extent to which this hybrid definition contributes to the potential diachroneity remains unclear, but it introduces additional uncertainty into the results.

It is however important to emphasize that these results are based on a reconnaissance scale dataset and that significant inconsistencies remain to be fully explained (e.g. the disagreement between the Kvabebi and Sarica sections). The results nonetheless strongly highlight the necessity of establishing local time scales in multiple locations within systems of interconnected basins, as previously suggested by prior work in the Paratethyan region (Vasiliev *et al.*, 2004; Krijgsman *et al.*, 2010; van Baak *et al.*, 2013) and more general results from basin and subbasin pairs (Brown *et al.*, 2005). It is indeed possible that the disparity between the previous results from Kvabebi to those presented here for Sarica may be the product of extremely local effects, a hypothesis that can only be tested with continued, rigorous dating of sections within the Kura–Caspian system.

Our results do not directly suggest that other Caspian regional stage boundaries besides the Productive Series – Akchagyl are diachronous, but it reasonable that other stage boundaries could be similarly diachronous between the interior of the Kura Basin and the margins of the South Caspian Basin. Because the Caspian regional stages are dually defined biostratigraphically and in terms of changes in Caspian base level, from a sequence stratigraphic perspective, the stage boundary in any location is commonly a potentially highly diachronous sequence boundary or flooding surface (e.g. Mancini & Tew, 1997; Strong & Paola, 2008; Bhattacharya, 2011).

Implications for the Tectonic Evolution of the Greater Caucasus System

The new age constraints for the Productive Series–Akchagyl stage boundary also have implications for the proposed tectonic evolution of the eastern Greater Caucasus. Recent work suggests that during the Plio–Pleistocene, accommodation of active shortening within the eastern Greater Caucasus system shifted southward from the main range into the foreland, forming the Kura fold-thrust belt, within which the Vashlovani and Sarica sections are exposed (Fig 1., Forte *et al.*, 2010, 2013). The initiation ages for the Kura fold-thrust belt structures and similar structures offshore in the South Caspian Basin, and thus the timing of the structural reorganization within the Greater Caucasus system, has primarily been determined by assessing whether particular units were deposited syn- or pretectonically (e.g. Devlin *et al.*, 1999; Forte *et al.*, 2010, 2013). In detail, Forte *et al.* (2010) used the observation that based on previous mapping, Akchagyl-aged strata in the western portion of the Kura fold-thrust belt appeared to be deposited syn-tectonically, whereas in the eastern portion of the fold-thrust belt they were likely deposited pretectonically, to argue for an eastward propagation of the fold-thrust belt through time. However, the results of this work, implying a westward younging of the Productive Series – Akchagyl stage boundary, suggest that this along-strike change in the pre- or syntectonic nature of the Akchagyl strata may be consistent with nearly synchronous along-strike initiation of the Kura fold-thrust belt, or at least, a less diachronous initiation of deformation along strike than originally suggested by Forte *et al.* (2010).

In addition, though not as striking as the changes in depositional environment driven by variations in Caspian base level, both the Sarica and Vashlovani sections record a general coarsening upwards seemingly independent of any trend in base level. We interpret this coarsening upwards to be caused by an increase in sediment input into these regions and likely increased gradients (i.e. relief) facilitating the transport of coarser material into the Kura Basin. The simplest explanation is that this increase in sediment input into the foreland is related to the growth of the Greater Caucasus Mountains, consistent with models and examples of stratigraphic responses to growing orogens (e.g. Burbank *et al.*, 1988; Heller *et al.*, 1988; Brozovic & Burbank, 2000; Allen *et al.*, 2013). However, clearly attributing this trend to a tectonic explanation requires detailed understanding of both the deformational and climatic history of the region (e.g. Ballato & Strecker, 2013). For example, a potentially important additional consideration is the role of alpine style glaciation in the Greater Caucasus, which began as earlier as *ca*. 3 Ma and continued throughout the Plio–Pleistocene (e.g. Milanovsky, 2000, 2008; Gobejishvili *et al.*, 2011), in influencing the sediment flux into the foreland. Similarly, the extent to which the large base-level drop during deposition of the Productive Series increased incision as previously suggested (e.g. Kvasov, 1964) and thus drove increased sediment input into the Kura basin also remains unclear. Unfortunately, the late Cenozoic deformation within the interior of the Greater Caucasus, absolute initiation age of structures within this portion of the Kura fold-thrust belt, and potential changes in regional

palaeo-climate all remain enigmatic, making detailed analysis of patterns within the stratigraphic record difficult at this time.

Implications for Stratigraphic Records in Subbasins

In general, our results suggest a potential for significant diachroneity, in the order of 0.5 Myrs, between stage boundary ages as measured in the interior of subbasins and main basins. It is unclear the extent to which the relative magnitude of this diachroneity depends on whether the sub- and main basin pair is internally or externally drained. However, we hypothesize that large, internally drained basins, like the Caspian, have the potential for much larger magnitudes of diachroneity in stage boundaries, similar to what we document here, because they have the potential for larger magnitudes of base-level change than basins whose base level is set by eustatic sea level (e.g. Fig. 2).

The potential for diachronous stage boundaries in internally drained subbasins also has implications for using the stratigraphic record to interpret structural or tectonic evolution of regions. Although internally drained basins can develop for many reasons, their formation is commonly mediated by structural controls (e.g. Carroll *et al.*, 2010) and thus many foreland basins experience periods of internal drainage. Similar to the case in the Kura basin and fold-thrust belt, unit or stage boundaries across which foreland strata are deposited pre- or syntectonically represents crucial constraints on the timing of deformation and initiation of structures (e.g. Burbank, 1983; Horton *et al.*, 2002; Casas-Sainz *et al.*, 2005). Significant diachroneity in these important stratigraphic boundaries in different regions of a foreland basin, depending on proximity to the main depocentre, thus has implications for understanding the relations between different structures, as we have suggested for the Kura fold-thrust belt. In detail, the scale of the observations and timeframe involved is of course crucial. For the Kura fold-thrust belt, because all of the structures are likely Plio-Pleistocene in age (Forte *et al.*, 2010, 2013), a diachroneity of a key stage boundary in the order of 0.5 Myrs is relevant, whereas with lower resolution and more protracted histories of fold-thrust belt formation, a diachroneity of this scale may not be important or recognizable.

If diachroneity of stage boundaries are more extreme in subbasins, then identifying whether a stratigraphic record was deposited in a sub- or main basin is important for interpreting these boundaries. While recognizing whether particular stratigraphic packages were deposited in a sub- or main basin environment is trivial in modern settings or with extensive subsurface data, this is not always the case in older stratigraphic environments. The example from the Kura and South Caspian basins suggest that extreme diversity in accumulation rates across a single unit may be diagnostic for recognizing sub- and main basins in the stratigraphic record. In this example, Productive Series strata in the South Caspian Basin are estimated to be 6 km thick (e.g. Allen *et al.*, 2002), which paired with a duration of 2.4 Myr for the Productive Series from the Lokbatan section (Fig. 2) suggests an average accumulation rate, not accounting for compaction, of *ca.* 250 cm kyr^{-1}. In contrast, based on our correlations, the Productive Series is *ca.* 150 m thick in Vashlovani and a minimum of *ca.* 210 m thick in Sarica. Using the duration of Productive Series deposition in Lokbatan yields accumulation rates *ca.* 6 and *ca.* 9 cm kyr^{-1} for Vashlovani and Sarica respectively. Considering the proposed extended duration of the Productive Series, we present here for the interior of the Kura Basin and using 2.7 Ma as the end of the Productive Series, lowers these accumulation rates to 5 and *ca.* 7 cm kyr^{-1} respectively. Even without the shorter duration of the Productive Series in the interior of the Kura Basin, the accumulation rates in the subbasin environment vs. the main basin are two orders of magnitude lower.

Contrasting this with comparisons between the thickness of the Akchagyl in the Kura and South Caspian basins suggests a much less apparent variation between these two locations. In the South Caspian basin, the Akchagyl is estimated to be 450 m thick (Allen *et al.*, 2002). This is comparable to the *ca.* 250 m of Akchagyl present at Vashlovani, using the base of unit V3 and the approximate location of the Akchagyl-Apsheron contact within unit V3 from Abdullaev *et al.*, (1957), and the *ca.* 300 m of Akchagyl at Sarica. Calculating accumulation rates for the Akchagyl is problematic as the age of the Akchagyl–Apsheron contact remains unclear (e.g. van Baak *et al.*, 2013), but the similarity of the thicknesses between the South Caspian and Kura basins suggests a relative similarity in accumulation rates. Importantly, the Productive Series represents deposition during a low-stand in the Caspian system whereas the Akchagyl was deposited during a high-stand, suggesting that for the purposes of identifying which portions of a stratigraphic section were deposited in a sub- vs. main basin, low-stand deposits may be more useful. Importantly though, these results may be influenced by the sparseness of this dataset and higher resolution studies utilizing seismic data across sub- and main basin pairs document extremely complicated and spatially variable patterns of deposition and nondeposition during low-stands (e.g. Munteanu *et al.*, 2012).

CONCLUSIONS

Our new stratigraphic results within the interior of the Kura Basin indicates that in detail, the Akchagyl transgression was likely a diachronous event with Akchagyl strata appearing at minimum 0.5 Myr later in the western Kura Basin than in the South Caspian Basin. This highlights the potential for significant local diachroneity in the age of regional stage boundaries between subbasins and main basins and the necessity of establishing local time scales in various parts of sub- and main basin pairs.

Regionally, the diachroneity of the Akchagyl transgression has important implications for the tectonic history of the region, because the Akchagyl sediments are a distinctive marker horizon and have previously been used to constrain the initiation age of Plio-Pleistocene structures within the Kura fold-thrust belt (e.g. Forte *et al.*, 2010). These results call into question the degree to which this fold-thrust belt records an eastward propagation. Future work should focus on more detailed, local chronologies of key strata to better constrain potential along-strike patterns in initiation ages to further evaluate the hypothesis of an eastward propagating Kura fold-thrust belt. The example of the Kura and South Caspian basins represent an interesting analogue for studying the interplay of tectonics and climatically mediated base level in a sub- and main basin pair. Preliminary results suggest that high spatial variability in low-stand deposits, as exemplified by the Productive Series in this region, may be evidence of the existence of sub and main basins in older stratigraphic records where the first-order basin geometry is not as clear as in modern examples or in areas with extensive subsurface data.

ACKNOWLEDGEMENTS

We thank Zak Murtuzayev, Tea Mumladze, Ana Menabde and David Kandelaki for their assistance in the field. An early version of this manuscript benefited from suggestions by Scott Bennett and Austin Elliott. We are additionally very thankful for beneficial discussions on the intricacies of the Caspian time scale with Christiaan van Baak and for him providing us a copy of the Lokbatan measured section. Helpful comments by editor Christopher Jackson and reviewers Cari Johnson and Paolo Ballato greatly improved this manuscript. This material is based upon work supported by the National Science Foundation under Grant No. 0810285. Additional funding was provided to A.M.F. from the UC Davis Department of Geology Cordell Durrell Fund and the Geological Society of America.

SUPPORTING INFORMATION

Additional Supporting Information may be found in the online version of this article:

Appendix S1. Facies associations.

Appendix S2. Micropalaeontology results

Figure S1. 1–3. *Candoniella formosa* (Livental); 1, 2. LV, external lateral view; 3. RV., internal view; 4. *Candona albicans* (Brady) (possible to be considered now as juvenile of *Pseudocandona* sp.), RV, external lateral view; 5, 7. *Caspiocypris* ex. gr. *filona* (Livental), juveniles, all RV., external lateral view; 8. Eucypris sp., lateral view of fragmented shells, possible juvenile of *Eucypris crassa* Müller; 9. *Ilyocypris* sp., fragmented shell.

Figure S2. 1–4. *Ammonia beccarii* (Linné); 5, 6. *Miliolina* sp.; 7–13. *Cyprideis torosa* (Jones); 7,8. RV, external lateral view; 9. Carapace, lateral view from the RV; 10. LV, external lateral view; 11, 12. RV, external lateral view, juveniles; 13. Carapace, dorsal view; 14, 15. *Limnocythere* ex. gr. *alveolata* Suzin, RV. lateral external view; 16. *Ilyocypris bradyi* Sars, LV, external lateral view; 17. *Candona* sp., possible juvenile of *Candona neglecta* Sars, RV, external lateral view; 18, 19. *Hydrobia syrmica* Neumayr.

Figure S3. 1–4. *Ammonia beccarii* (Linné); 5–9. *Cyprideis torosa* (Jones); 5, 6. LV, lateral external view; 7. RV, external lateral view, male; 8, 9. RV, external lateral view, females; 10–14. *Loxoconcha laevatula* Livental; 10,11. RV, lateral external view, males; 12, 13. RV, lateral external view, femals; 14, RV, internal view, female; 15, 16. *Amnicythere gubkini* Livental; 15. LV, external lateral view; 16. RV, external lateral view; 17, 18. *Hydrobia syrmica* Neumayr.

Figure S4. 1–7. *Cyprideis torosa* (Jones), with smooth shell, forma *littoralis*; 1. LV, external lateral view, male; 2. RV, external lateral view, male; 3, 5. Carapace, lateral view from the RV, female; 4. LV, external lateral view, female; 6. LV, internal view, female; 7. Crapace, dorsal view; 8–15. *Loxoconcha eichwaldi* Livental var. *tuberculata*; 8. LV, external lateral view, male; 9. RV, external lateral view, male; 10. Carapace, lateral view from RV, male; 11. LV, external lateral view, female; 12. Carapace, lateral view from RV, female; 13. LV, internal view, female; 14. Carapace, dorsal view, female; 15. Carapace, ventral view, female; 16–21. *Loxoconcha petasus* Livental; 16. LV, external lateral view, male; 17, 18. RV, external lateral view, male; 19. LV, extenal lateral view, female; 20. RV, external alteral view, female; 21. RV, internal view, male; 22–25. *Loxoconcha* ex. gr. *eichwaldi* Livental; 22. LV, external lateral view, male; 23. RV, external lateral view, male; 24. LV, external lateral view, female; 25. RV, external lateral view, female; 26–31. *Amnicythere* ex. gr. *gubkini* Livental; 26, 28. LV, external lateral view; 27. RV, external lateral view; 29. Carapace, view from the RV; 30. Carapace, dorsal view; 31, Carapace, ventral view; 32, 33. *Candona* ex. gr. *angulata* G. W. Müller; 32. Carapace, lateral view from the LV, male; 33. Carapace, lateral view from the RV, male; 34, 35. *Hydrobia* ex. gr *syrmica* Neumayr.

Table S1. U-Pb geochronologic analyses.

REFERENCES

Abdullaev, R.N., Agabekov, M.G. & Gavrilov, M.D. (1957) K-38-XXIX. Geological Map of the USSR. Scale 1:200,000. Ministry of Geology and Conservation of Mineral Resources of the USSR, Moscow.

Abreu, V. & Nummedal, D. (2007) Miocene to quaternary sequence stratigraphy of the South and Central Caspian Basins. In: *Oil and Gas of the Greater Capsian Area* (Ed. by Yilmaz P.O. & Isaken G.H.), *AAPG Stud. Geology*, **55**, 65–86.

Agustí, J., Vekua, A., Oms, O., Lordkipanidze, D., Bukhsianidze, M., Kiladze, G. & Rook, L. (2009) The Pliocene-Pleistocene succession of Kvabebi (Georgia) and the back-

ground to the early human occupation of Southern Caucasus. *Quatern. Sci. Rev.*, **28**, 3275–3280.

Aliyeva, E.G.-M. (2005) Reservoirs of the lower Pliocene productive series at the western flank of the south Caspian basin. *Lithol. Min. Resour.*, **40**, 267–278.

Ali-Zade, A.A. (2005) Geological Map of Azerbaijan Republic. Scale 1:500,000. National Academy of Sciences of Azerbaijan Republic Geology Institute, Baku, Azerbaijan.

Allen, J.L. & Johnson, C.L. (2011) Architecture and formation of transgressive-regressive cycles in marginal marine strata of the John Henry Member, Straight Cliffs Formation, Upper Cretaceous of Southern Utah, USA. *Sedimentology*, **58**, 1486–1513.

Allen, M.B., Jones, S., Ismail-Zadeh, A., Simmons, M. & Anderson, L. (2002) Onset of subduction as the cause of rapid Pliocene-Quaternary subsidence in the South Caspian Basin. *Geology*, **30**, 775–778.

Allen, M.B., Vincent, S.J., Alsop, G.I., Ismail-Zadeh, A. & Flecker, R. (2003) Late Cenozoic deformation in the South Caspian Region: effects of a rigid basement block within a collision zone. *Tectonophysics*, **366**, 223–239.

Allen, P.A., Armitage, J.J., Carter, A., Duller, R.A., Michael, N., Sinclair, H.D., Whitchurch, A.L. & Whittaker, A.C. (2013) The Qs problem: sediment volumetric balance of proximal foreland basin systems. *Sedimentology*, **60**, 102–130.

Andersen, T. (2005) Detrital zircons as tracers of sedimentary provenance: limiting conditions from statistics and numerical simulation. *Chem. Geol.*, **216**, 249–270.

Avdeev, B. & Niemi, N.A. (2011) Rapid Pliocene exhumation of the central Greater Caucasus constrained by low-temperature thermochronometry. *Tectonics*, **30**, TC2009.

Azizbekov, S.A. (ed.) (1972) *Azerbaijan Ssr (in Russian)*. Geology of the USSR. Nauka, Moscow.

van Baak, C.G.C. (2010) *Glacio-Marine Transgressions of the Early and Middle Pleistocene Caspian Basin, Azerbaijan*. Utrecht University, Utrecht, the Netherlands.

van Baak, C.G.C., Vasiliev, I., Stoica, M., Kuiper, K.F., Forte, A.M., Aliyeva, E. & Krijgsman, W. (2013) A magnetostratigraphic time frame for Plio-Pleistocene transgressions in the South Caspian Basin, Azerbaijan. *Global Planet. Change*, **103**, 119–134.

Ballato, P. & Strecker, M.R. (2013) Assessing tectonic and climatic causal mechanisms in foreland-basin stratal architecture: insights from the Alborz Mountains, northern Iran. *Earth Surf. Proc. Land.*, **39**, 110–125.

Bhattacharya, J.P. (2011) Practical problems in the application of the sequence stratigraphic method and key surfaces: integrating observations from ancient fluvial-deltaic wedges with Quaternary and modelling studies. *Sedimentology*, **58**, 120–169.

Blum, M.D. & Törnqvist, T.E. (2000) Fluvial repsonse to climate and sea-level change: a review and look forward. *Sedimentology*, **47**, 2–48.

Boomer, I., Guichard, F. & Lericolais, G. (2010) Late Pleistocene to Recent ostracod assemblages from the western Black Sea. *J. Micropalaeontol*, **29**, 119–133.

Brown, L.F., Loucks, R.G. & Trevino, R.H. (2005) Site-specific sequence-stratigraphic section benchmark charts are key to regional chronostratigraphic systems tract analysis in growth-faulted basins. *Am. Assoc. Pet. Geol. Bull.*, **89**, 715–724.

Brozovic, N. & Burbank, D. (2000) Dynamic fluvial systems and gravel progradation in the Himalayan foreland. *Geol. Soc. Am. Bull.*, **112**, 394–412.

Burbank, D. (1983) The chronology of inermontane-basin development in the northwestern Himalaya and the evolution of the Northwest Syntaxis. *Earth Planet. Sci. Lett.*, **64**, 77–92.

Burbank, D., Beck, R.A., Raynolds, R.G.H., Hobbs, R.S. & Tahirkheli, R.A.K. (1988) Thrusting and gravel progradation in foreland basins: a test of post-thrusting gravel dispersal. *Geology*, **16**, 1143–1146.

Carroll, A.R., Graham, S.A. & Smith, M.E. (2010) Walled sedimentary basins of China. *Basin Res.*, **22**, 17–32.

Carter, R.M., Fulthorpe, C.S. & Naish, T.R. (1998) Sequence concepts at seismic and outcrop scale: the distinction between physical and conceptual stratigraphic surfaces. *Sed. Geol.*, **122**, 165–179.

Casas-Sainz, A.M., Soto-Marin, R., Gonzalez, A. & Villalain, J.J. (2005) Folded onlap geometries: implications for recognition of syn-sedimentary folds. *J. Struct. Geol.*, **27**, 1644–1657.

Catuneanu, O. (2002) Sequence stratigraphy of clastic systems: concepts, merits, and pitfalls. *J. Afr. Earth Sc.*, **35**, 1–43.

Catuneanu, O., Willis, A.J. & Miall, A.D. (1998) Temporal significance of sequence boundaries. *Sed. Geol.*, **121**, 157–178.

Devlin, W.J., Cogswell, J.M., Gaskins, G.M., Isaken, G.H., Picther, D.M., Puls, D.P., Stanely, K.O. & Wall, G.R.T. (1999) South Caspian basin: young, cool, and full of promise. *GSA Today*, **9**, 1–9.

Dumont, H.J. (1998) The Caspian Lake: history, biota, structure, and function. *Limnol. Oceanogr.*, **43**, 44–52.

Fielding, C.R., Ashworth, P.J., Best, J.L., Prokocki, E.W. & Sambrook Smith, G.H. (2012) Tributary, distributary and other fluvial patterns: what really represents the norm in the continental rock record? *Sed. Geol.*, **261–262**, 15–32.

Forte, A.M. (2012) *Late Cenozoic Evolution of the Greater Caucasus Mountains and Kura Foreland Basin: Implications for Early Orogenesis*. University of California, Davis.

Forte, A.M. & Cowgill, E. (2013) Late Cenozoic base-level variations of the Caspian Sea: a new review of its history and proposed driving mechansims. *Palaeogeogr. Palaeoclimatol. Palaeoecol.*, **386**, 392–407.

Forte, A.M., Cowgill, E., Bernardin, T., Kreylos, O. & Hamann, B. (2010) Late Cenozoic deformation of the Kura fold-thrust belt, southern Greater Caucasus. *Geol. Soc. Am. Bull.*, **122**, 465–486.

Forte, A.M., Cowgill, E., Murtuzayev, I., Kangarli, T. & Stoica, M. (2013) Structual geometries and magnitude of shortening in the eastern Kura fold-thrust belt, Azerbaijan: implications for the development of the Greater Caucasus Mountains. *Tectonics*, **32**, Doi: 10.1002/tect.20032.

Gehrels, G.E. (2012) Detrital zircon U-Pb geochronology: current methods and new opportunties. In: *Recent Advances in Tectonics of Sedimentary Basins* (Ed. by C.J. Busby & A. Azor), pp. 47–62. Blackwell Publishing, West Sussex, UK.

Gehrels, G.E., Valencia, V. & Ruiz, J. (2008) Enhanced precision, accuracy, efficiency, and spatial resoultion of U-Pb ages by laser ablation-multicollector-inductively coupled plasma-mass spectrometry. *Geochem. Geophys. Geosyst.*, **9**, Q03017.

Gobejishvili, R., Lomidze, N. & Tielidze, L. (2011) Late Pleistocene (WÜrmian) Glaciations of the Caucasus. In: *Quaternary Glaciations – Extent and Chronology* (Ed. by Ehlers J., Gibbard P. L. & Hughes P.D.), *Dev. Quarter. Sci.*, **15**, 141–147. Elsevier, Amsterdam.

Gradstein, F.M., Ogg, J.G., Schmitz, M. & Ogg, G. (eds.) (2012) *The Geologic Time Scale 2012*. Elsevier, Amsterdam.

Green, T., Abdullayev, N., Hossack, J., Riley, G. & Roberts, A.M. (2009) Sedimentation and subsidence in the south Caspian Basin, Azerbaijan. In: *South Caspian to Central Iran Basins* (Ed. by Brunet M.-F., Wilmsen M. & Granath J.W.), *Geol. Soc.*, **312**, 241–260.

Gudjabidze, G.E. (2003) Geological map of Georgia. Scale 1:500,000 (Ed. by I.P. Gamkrelidze, G.N. Abesadze, V.I. Buadze, T.V. Djanelidze, O.Z. Dudauri, D.N. Kandelaki, G.S. Nadareishvili, D. Papava, M.P. Pruidze, D.M. Shengelia & M.V. Topchishvili), Georgian State Department of Geology and National Oil Company, Tbilisi, Georgia.

Haq, B.U., Hardenbol, J. & Vail, P.R. (1987) Chronology of fluctuating sea levels since the Triassic. *Science*, **235**, 1156–1167.

Heller, P.L., Angevine, C.L., Winslow, N.S. & Paola, C. (1988) Two-phase stratigraphic model of foreland-basin sequences. *Geology*, **16**, 501–504.

Hinds, D.J., Aliyeva, E., Allen, M.B., Davies, C.E., Kroonenberg, S.B., Simmons, M. & Vincent, S.J. (2004) Sedimentation in a discharge dominated fluvial-lacustrine system: the Neogene Productive Series of the South Caspian Basin, Azerbaijan. *Mar. Pet. Geol.*, **21**, 613–638.

van Hinte, J.E. (1978) Geohistory analysis – application of micropaleontology in exploration geology. *Am. Assoc. Pet. Geol. Bull.*, **62**, 201–222.

Hoogendoorn, R.M., Boels, J.F., Kroonenberg, S.B., Simmons, M., Aliyeva, E., Babazadeh, A.D. & Huseynov, D. (2005) Development of the Kura delta, Azerbaijan; a record of Holocene Caspian sea-level changes. *Mar. Geol.*, **222–223**, 359–380.

Horton, B.K., Yin, A., Spurlin, M.S., Zhou, J. & Wang, J. (2002) Paleocene-Eocene syncontractional sedimentation in narrow, lacustrine-dominated basins of east-central Tibet. *Geol. Soc. Am. Bull.*, **114**, 771–786.

Immenhauser, A. (2009) Estimating palaeo-water depth from the physical rock record. *Earth Sci. Rev.*, **96**, 107–139.

Inan, S., Yalcin, M.N., Guliev, I., Kuliev, K. & Feizullayev, A.A. (1997) Deep petroleum occurrences in the Lower Kura Depression, South Caspian Basin, Azerbaijan: an organic geochemical and basin modeling study. *Mar. Pet. Geol.*, **14**, 731–762.

Isaneva, M.L. & Sadngova, T.D. (1999) Paleogeography and paleotectonics of western Azerbaijan during upper pliocene and pleistocene time. *Geophysics News in Azerbaijan*, **2**.

Jackson, J., Priestly, K., Allen, M.B. & Berberian, M. (2002) Active tectonics of the south Caspian basin. *Geophys. J. Int.*, **148**, 214–245.

Jones, R.W. & Simmons, M. (1996) A review of the stratigraphy of Eastern Paratethys (Oligocene-Holocene). *Bull. Nat. Hist. Mus. Lond.*, **52**, 25–49.

Karpytchiev, Y.A. (1993) Reconstruction of Caspian Sea-level fluctuations: radiocarbon dating coastal and bottom deposits. *Radiocarbon*, **35**, 409–420.

Kizlov, A. & Toropov, P. (2007) East European river runoff and Black Sea and Caspian Sea level changes as simulated within the Paleoclimate modeling intercomparison project. *Quatern. Int.*, **167–168**, 40–48.

Kozhevnikova, I.A. & Shveikina, V.I. (2008) Nonlinear dynamics of level variations in the Caspian Sea. *Water Resour.*, **35**, 297–304.

Krijgsman, W., Stoica, M., Vasiliev, I. & Popov, V.V. (2010) Rise and fall of the Paratethys Sea During the Messinian Salinity Crisis. *Earth Planet. Sci. Lett.*, **290**, 183–191.

Kroonenberg, S.B., Rusakov, G.V. & Svitoch, A.A. (1997) The wandering of the Volga Delta: a response to rapid Caspian sea-level change. *Sed. Geol.*, **107**, 189–209.

Kroonenberg, S.B., Alekseevski, N.I., Aliyeva, E., Allen, M.B., Aybulatov, D.N., Baba-Zadeh, A., Badyukova, E.N., Davies, C.E., Hinds, D.J., Hoogendoorn, R.M., Huseynov, D., Ibrahimov, B., Mamedov, P., Overeem, I., Rusakov, G.V., Suleymanova, S.F., Svitoch, A.A. & Vincent, S.J. (2005) Two Deltas, Two Basins, One River, One Sea: the modern Volga Delta as an analogue for the Neogene productive series, South Caspian Basin. In: *River Deltas-Concepts, Models, and Examples* (Ed. by, Giosan, L. & Bhattacharya, J.P.). SEPM Special Publications,), pp. 231–256, Society for Sedimentary Geology (SEPM), Tulsa, OK.

Kvasov, D.D. (1964) Middle Pliocene hydrology of the Caspian. *Dokl. Earth Sci.*, **158**, 39–41.

Kvasov, D.D. (1983) Causes of the marked regression of the Black and Caspian Seas about five million years ago. *Oceanology*, **23**, 331–335.

Li, C.X., Ivanov, V., Fan, D.D., Korotaev, V., Yang, S.Y., Chalov, R. & Liu, S.G. (2004) Development of the Volga Delta in response to Caspian Sea-level fluctuation during last 100 years. *J. Coastal Res.*, **20**, 401–414.

Liu, K., Liang, T.C.K., Paterson, L. & Kendall, C.G.S.C. (1998) Computer simulation of the influence of basin physiography on condensed section deposition and maximum flooding. *Sed. Geol.*, **122**, 181–191.

Liu, J.G., Mason, P.J., Clerici, N., Chen, S., Davis, A., Miao, F., Deng, H. & Liang, L. (2004) Landslide hazard assessment in the Three Gorges area of the Yangtze river Using Aster imagery: Zigui-Badong. *Geomorphology*, **61**, 171–187.

Mamedov, A.V. (1973) *Geological Structure of the Mid-Kura Depression (in Russian)*. Elm, Baku.

Mamedov, A.V. (1997) The late pleistocene-holocene history of the Caspain sea. *Quatern. Int.*, **41**(42), 161–166.

Mancini, E.A. & Tew, B.H. (1997) Recognition of maximum flooding events in mixed siliciclastic-carbonate systems: key to global chronostratigraphic correlation. *Geology*, **25**, 351–354.

Martin, J., Paola, C., Abreu, V., Neal, J. & Sheets, B. (2009) Sequence stratigraphy of experimental strata under known conditions of differential subsidence and variable base level. *Am. Assoc. Pet. Geol. Bull.*, **93**, 503–533.

Matoshko, A.V., Gozhik, P.F. & Danukalova, G. (2004) Key Late Cenozoic fluvial archives of eastern Europe: the Dniester, Dnieper, Don and Volga. *Proc. Geol. Assoc.*, **115**, 141–173.

Menabde, I.V., Svitoch, A.A. & Yanina, T.A. (1993) Changes in Caspian Salinity during the Pleistocene (According to Data of an Analysis of Malacofauna). *Water Resour.*, **19**, 303–307.

Miall, A.D. (1977) A review of the braided-river depositional environment. *Earth Sci. Rev.*, **13**, 1–62.

Milanovsky, E. (2000) The Plio-Pleistocene glaciation in eastern Europe, Siberia, and the Caucasus: evolution of thoughts. *Eclogae Geol. Helv.*, **93**, 379–394.

Milanovsky, E. (2008) Origin and development of ideas on Pliocene and Quaternary glaciations in northern and eastern Europe, Iceland, Caucasus and Siberia. In: *History of Geomorphology and Quaternary Geology* (Ed. by Grapes R., Oldroyd D. & Grigelis A.) *Geol. Soc. Lond.*, **301**, 87–115.

Miller, K.G., Mountain, G.S., Wright, J.D. & Browning, J.V. (2011) A 180-million-year record of sea level and ice volume variations from continental margins and deep-sea isotopic records. *Oceanography*, **24**, 40–53.

Munteanu, I., Matenco, L., Dinu, C. & Cloetingh, S. (2012) Effects of large sea-level variations in connected basins: the Dacian-Black Sea system of the Eastern Paratethys. *Basin Res.*, **24**, 583–597.

Nalivkin, D.V. (1973) The Mediterranean geosyncline. In: *Geology of the U.S.S.R. (English Translation)* (Ed. by D.V. Nalivkin), pp. 578–685. Oliver and Boyd, Edinburgh.

Nalivkin, D.V. (1976) Geologic Map of the Caucasus (in Russian). scale 1:500,000. Ministry of Geology, USSR, Moscow.

Nichols, G.J. & Fisher, J.A. (2007) Processes, facies and architecture of fluvial distributary system deposits. *Sed. Geol.*, **195**, 75–90.

Nichols, G.J. & Hirst, J.P. (1998) Alluvial fans and fluvial distributary systems, Oligo-Miocene, northern Spain: contrasting processes and products. *J. Sediment. Res.*, **68**, 879–889.

Overeem, I., Kroonenberg, S.B., Veldkamp, A., Groenesteijn, K., Rusakov, G.V. & Svitoch, A.A. (2003a) Small-scale stratigraphy in a large ramp delta: recent and Holocene sedimentation in the Volga Delta, Caspian Sea. *Sed. Geol.*, **159**, 133–157.

Overeem, I., Veldkamp, A., Tebbens, L. & Kroonenberg, S.B. (2003b) Modelling Holocene stratigraphy and depocentre migration of the Volga Delta due to Caspian Sea-level change. *Sed. Geol.*, **159**, 159–175.

Popov, S.V., Shcherba, I.G., Ilyina, L.B., Nevesskaya, L.A., Paramonova, N.P., Khondkarian, S.O. & Magyar, I. (2006) Late Miocene to Pliocene palaeogeography of the Paratethys and Its relation to the Mediterranean. *Palaeogeogr. Palaeoclimatol. Palaeoecol.*, **238**, 91–106.

Popov, S.V., Antipov, M.P., Zastroshnov, A.S., Kurina, E.E. & Pinchuk, T.N. (2010) Sea-level fluctuations on the northern shelf of the Eastern Paratethys in the Oligocene-Neogene. *Stratigr. Geol. Correl.*, **18**, 200–224.

Reynolds, A.D., Simmons, M., Bowman, M.B.J., Henton, J., Brayshaw, A.C., Ali-Zade, A.A., Guliyev, I.S., Suleymanova, S.F., Ateava, E.Z., Mamedova, D.N. & Koshkarly, R.O. (1998) Implications of outrcrop geology for reservoirs in the Neogene Productive Series: Apsheron Peninsula, Azerbaijan. *Am. Assoc. Pet. Geol. Bull.*, **82**, 25–49.

Rumyantsev, V.A., Rumyanstev, A.O. & Trapeznikov, Y.A. (2008) The nonstationary and nonlinear character of Caspian Sea level variations. *Water Resour.*, **35**, 185–190.

Rychagov, G.I. (1997) Holocene oscillations of the Caspain Sea, and forecasts based on paleogeographical reconstructions. *Quatern. Int.*, **41**(42), 167–172.

Sedletskii, V.S. & Baikov, A.A. (1997) The nature of Caspian Sea level functions. *Lithol. Min. Resour.*, **32**, 208–215.

Shanley, K.W. & McCabe, P.J. (1994) Perspectives on the sequence stratigraphy of continental strata: report of a Working Group at the 1991 Nuna Conference on High Resolution Sequence Stratigraphy. *Am. Assoc. Pet. Geol. Bull.*, **74**, 544–568.

Shirinov, F.A. & Bajenov, Y.P. (1962) *Geological Structure of the Southern Foothills of the Greater Caucasus (in Russian)*. Azerneshr, Baku.

Steenwinkel, M.V. (1990) Sequence stratigraphy from "spot" outcrops – example from a carbonate-dominated setting: devonian-carboniferous transition, Dinant syncinorium (Belgium). *Sed. Geol.*, **69**, 259–280.

Stoica, M., Lazar, I., Krijgsman, W., Vasiliev, I., Jipa, D.C. & Floroiu, A. (2013) Paleoenvironmental evolution of the East Carpathian foredeep during the late Miocene-early Pliocene (Dacian Basin; Romania). *Global Planet. Change*, **103**, 135–148.

Strong, N. & Paola, C. (2008) Valleys that never were: time surfaces versus stratigraphic surfaces. *J. Sediment. Res.*, **78**, 579–593.

Svitoch, A.A. (1999) Caspian Sea Level in the Pleistocene: heirarchy and position in the paleogeographic and chronological records. *Oceanology*, **39**, 94–101.

Svitoch, A.A., Selivanov, A.O. & Yanina, T.A. (2000) The Pont-Caspian and Mediterranean basins in the Pleistocene (paleogeography and correlation). *Oceanology*, **40**, 868–881.

Van Wagoner, J.C. & Bertram, G.T. (eds.) (1995) *Sequence Stratigraphy of Foreland Basin Deposits*. Aapg Memoir. American Association of Petroleum Geologists, Tulsa, OK.

Vasiliev, I., Krijgsman, W., Langereis, C.G., Panaiotu, C.E., Matenco, L. & Bertotti, G. (2004) Towards an astrochronological framework for the eastern Paratethys Mio-Pliocene sedimentary sequences of the Foscani basin (Romania). *Earth Planet. Sci. Lett.*, **227**, 231–247.

Vasiliev, I., Krijgsman, W., Stoica, M. & Langereis, C.G. (2005) Mio-Pliocene magnetostratigraphy in the southern Carpathian foredeep and Mediterranean-Paratethys correlations. *Terra Nova*, **17**, 376–384.

Vasiliev, I., Reichart, G.-J., Davies, G.R., Krijgsman, W. & Stoica, M. (2010) Strontium isotope ratios of the Eastern Paratethys during the Mio-Pliocene transition: implications for interbasinal connectivity. *Earth Planet. Sci. Lett.*, **292**, 123–131.

Vermeesch, P. (2004) How many grains are needed for a provenance study? *Earth Planet. Sci. Lett.*, **224**, 441–451.

Vincent, S.J., Davies, C.E., Richards, K. & Aliyeva, E. (2010) Contrasting Pliocene fluvial depostional systems within the rapidly subsiding South Caspian basin: a case study of the palaeo-Volga and palaeo-Kura river systems in the Surakhany Suite, Upper Productive Series, onshore Azerbaijan. *Mar. Pet. Geol.*, **27**, 2079–2106.

Zubakov, V.A. (1988) Climatostratigraphic scheme of the Black Sea Pleistocene and its correlation with the oxygen-isotope scale and glacial events. *Quatern. Res.*, **29**, 1–24.

Zubakov, V.A. (1992) Chronostratigraphic correlation of the ponto-Caspian and Mediterranean Pliocene and terminal Miocene. *Paleontologia. I Evolucio.*, **24–25**, 79–89.

Zubakov, V.A. (2001) History and causes of variations in the Caspian Sea level: the Miopliocene, 7.1–1.95 million years ago. *Water Resour.*, **28**, 249–256.

Zubakov, V.A. & Borzenkova, I.I. (1990) *Global Palaeoclimate of the Late Cenozoic*. Elsevier, Amsterdam.

Manuscript received 21 August 2013; In revised form 13 February 2014; Manuscript accepted 19 February 2014.

Appendix S1 - Facies Associations

S1.1. Unlaminated Silt and Clay Facies

Unlaminated silt and clay facies is also predominantly fine grained with greater than 10% silt intermixed with clay. Two dominant lithologies are present within the unlaminated silt and clay facies, clayey-silt (defined as between 10 and 50% silt) and silty-clay (defined as between 50% and 90% silt). Fresh surfaces of clayey-silts commonly have a tan-grey mottled color, whereas silty clays are a more uniform tan to buff color. Both are typically unlaminated and relatively homogenous, but in some cases, the silty-clays consist of mm-scale interbeds of silts and clays. Both macro- and micro-fauna are common in unlaminated silt and clay facies with mixtures of whole and fragmented skeletal grains, derived predominantly from bivalves and gastropods. Rare burrows are preserved. Fossil plant material is common, including leaf impressions and sections of semi-petrified wood ranging in size from a few millimeters to several centimeters long. Particular horizons composed of unlaminated silt and clay facies also contain abundant coal seams, coal roots in life position, and branches and fragments of coal. Preserved soil carbonate crusts and rhizoliths are also present in some unlaminated silt and clay facies and some strata preserve mud cracks. The unlaminated silt and clay facies contains abundant evidence for periodic subaerial exposure. The typical lack of lamination suggests extensive bioturbation, also consistent with the general abundance of macro fauna found in these deposits. The predominance of fossil assemblages in unlaminated silt and clay facies and the lack of these fauna in fluvial dominated facies described below suggest that unlaminated silt and clay facies likely accumulated in

shallow ephemeral ponds or lakes, however they could represent distal overbank and floodplain deposits.

S1.2. Massive Silt Facies

The massive silt facies consists predominantly of silts and fine sand that may grade into clay and silty-clay. Massive silt facies commonly contains centimeter scale interbedding of laminated siltstones and more clay-rich horizons. The rest of the massive silt facies lacks sedimentary structures. Fossils are rare to absent. The massive silt facies under- or overlies coarser sand or conglomeratic facies. Massive silt facies is interpreted as being deposited on the floodplain of fluvial systems, relatively proximal to river channels.

S1.3. Cross-stratified Sand and Gravel Facies

Cross-stratified sand and gravel facies are mostly composed of sands with isolated conglomerates. Cross-stratified sands and gravel facies commonly have erosive, scoured contacts with underlying strata and are normally graded with pebble-conglomerates or coarse sands grading upwards to fine sands and silts. In contrast, a small percentage of cross-stratified sands and gravel facies have conformable contacts at their base with relatively fine grained sand grading to coarser sand at the center of the deposit and then normal grading upwards, back to fine grained sand at their tops. Most cross-stratified sands and gravel facies are laterally continuous for at least several hundred meters, but commonly display thickness variations along strike. Rarely, cross-stratified sands and gravel facies occur as isolated meter-thick and 2-5 meter-wide deposits with preserved channel morphology.

The most common sedimentary features within cross-stratified sands and gravel facies are trough cross bedding, planar cross-stratification, and lenses of fossil concentrations. The trough cross bedding is usually sub-meter to meter scale, with individual troughs defined by grain size variations such as strings of pebbles within coarse-grained sandstone. Spacing between sets of planar cross-stratification is usually on the sub-meter scale, but in isolated locations occurs on a meter-scale. Fossil concentrations within the cross-stratified sands and gravel facies occur as several centimeter-thick graded beds, with the size of fragmented fossil pieces relatively uniform throughout but with a higher concentration of shells near the base. The fossil concentrations also commonly have an overall wavy morphology with wavelengths of several centimeters and wave heights of centimeter to millimeters. Intact fossils are rare within cross-stratified sands and gravel facies deposits, but where they do occur, they are typically larger grains such as mammalian bones or large pieces of petrified wood. In some locations, cross-stratified sands and gravel facies contain abundant mud-clast conglomerates. The mud-clasts range in size from pebbles to cobbles and are typically rounded to ellipsoid in shape. These mud-clasts commonly occur together with the meter scale planar cross-stratification, with strings of mud-clasts defining cross-stratification planes. Some cross-stratified sands and gravel facies deposits are devoid of any of these features and instead are massive sands with no internal sedimentary features.

Cross-stratified sands and gravel facies deposits are generally interpreted as fluvial channels, likely in meandering rivers or in a network of anastomosing or braided streams. Many of the sand and conglomerate bodies are extremely laterally continuous with only minimal change in thickness along their length suggestive of migration of

broad, shallow channels. Other cross-stratified sands and gravel facies deposits have clear channel morphologies, more consistent with channels abandoned during avulsion events in braided streams. We do not distinguish between meandering and braided fluvial facies because lack of exposure precluded lateral tracing of many of the deposits classified as cross-stratified sands and gravel facies, making the division between meandering and braided environments difficult.

S1.4. Massive Gravel Facies

The massive gravel facies is composed almost exclusively of conglomerate that locally contains isolated sand bodies. These deposits almost always have scoured bases, sometimes with upwards of a meter of relief over a few meters in along-strike distance. Most conglomerates are clast-supported, but isolated strata are matrix-supported. Clast sizes range from pebbles to boulders and are often poorly sorted. Clasts are typically, but not always, imbricated. Large packages of massive gravel facies contain isolated lenticular sand bodies, usually tens of centimeters in thickness and one to several meters in length. Massive gravel facies can also contain mud clasts near erosive bases, but unlike in the cross-stratified sands and gravel facies, these mud clasts typically have a very high axial-ratio and are generally millimeter to centimeter scale. Massive gravel facies also can contain meter-scale intervals of coarse sand horizons with occasional pebbles defining planar cross-stratification. Massive gravel facies are not typically graded (with some exceptions) and typically do not preserve channel geometries. Massive gravel facies are interpreted as being deposited in either braided fluvial systems or within alluvial fans. The matrix-supported horizons are likely debris flows deposits, more common in alluvial

fan settings, but otherwise distinguishing between braided fluvial and alluvial fan environments is difficult in this setting.

Appendix S2 – Micropaleontology Results

Here we present detailed descriptions of the assemblages from the Vashlovani section.

S2.1. Vashlovani

S2.1.1. Sample V-510 (Figure S1)

The sample contains only fresh water ostracods dominated by small sized candonidae species *Candoniella formosa* (Livental), now considered more likely as a juvenile of *Candona neglecta*, *Candona albicans* (Brady), possible also a juvenile of *Pseudocandona* sp., fragmented shells of *Eucypris crassa* Müller) and *Ilyocypris* sp., as well as a few juveniles of *Caspiocypris* ex. gr. *filona* (Livental). This ostracod assemblage suggests a fresh water environment. The age is difficult to define, because they are recorded in fresh water sediments from Upper Miocene of Paratethys and still alive in today fresh water lakes. Similar forms have been describes in Pleistocene (Apsheronian) sediments from Caspian and Black Sea areas as well from the "Productive Series" of Azerbaijan. (Agalarova *et al.*, 1961; Schornikov, 1964; Gofman, 1966; Vekua, 1975; Yassini, 1986; van Baak *et al.*, 2013).

S2.1.2. Sample V-1040 (Figure S2)

The sample contains brackish water foraminifers and ostracods. The foraminifera assemblage is dominated by *Ammonia beccarii* (Linné) associated with rare specimens of *Miliolina* sp. Ostracods are represented especially by *Cyprideis torosa* (Jones) together with few specimens of *Limnocythere* ex. gr. *alveolata* Suzin, *Ilyocypris bradyi* Sars and *Candona* sp. Microgastropod shells of *Hydrobia syrmica* Neumayr are also common in this sample. As a whole, the assemblage strongly indicates a brackish water environment. Similar microfauna assemblages are found in Lower Pleistocene (Apsheron) age sediments in both the Black Sea and Caspian Seas.

S2.1.3. Sample V-1260 (Figure S3)

The microfauna in this sample is dominated by *Ammonia beccarii* (Linné) and brackish water ostracods such as *Cyprideis torosa* (Jones), *Loxoconcha laevatula* Livental, *Amnicythere pediformis* (Schornikov) as well the brackish water microgastropod *Hydrobia syrmica* Neumayr. These faunal assemblages are common in Lower Pleistocene (Apsheron) in both the Black and Caspian Seas.

S2.1.4. Sample V-1465 (Figure S4)

This sample is very rich in well preserved brackish ostracod fauna dominated by *Cyprideis torosa* (Jones), with smooth shells, forma *littoralis*. This species is asociated with Loxoconchidae species *Loxoconcha eichwaldi* Livental, *L. eichwaldi* Livental var. *tuberculata*, *L. petasus* Livental and rare candonids like *Candona* ex. gr. *angulata* G. W. Müller. Hydrobiidae gastropods represented by *Hydrobia* ex. gr. *syrmica* Neumayr are also common as well some juvenile brackish water bivalves. These microfauna suggests a shallow brackish water environment, but the absence of foraminifers suggests that the water salinity was lower than in samples V-1040 and V-1260. These ostracod

associations were common during the Upper Pliocene to Pleistocene (Akchagyl to Apsheron) sediments from the Black and Caspian Seas.

Figure Captions

Figure S1

1-3. *Candoniella formosa* (Livental); 1, 2. LV, external lateral view; 3. RV., internal view; 4. *Candona albicans* (Brady) (possible to be considered now as juvenile of *Pseudocandona* sp.), RV, external lateral view; 5, 7. *Caspiocypris* ex. gr. *filona* (Livental), juveniles, all RV., external lateral view; 8. Eucypris sp., lateral view of fragmented shells, possible juvenile of *Eucypris crassa* Müller; 9. *Ilyocypris* sp., fragmented shell.

Figure S2

1-4. *Ammonia beccarii* (Linné); 5, 6. *Miliolina* sp.; 7-13. *Cyprideis torosa* (Jones); 7,8. RV, external lateral view; 9. Carapace, lateral view from the RV; 10. LV, external lateral view; 11, 12. RV, external lateral view, juveniles; 13. Carapace, dorsal view; 14. 15. *Limnocythere* ex. gr. *alveolata* Suzin, RV. lateral external view; 16. *Ilyocypris bradyi* Sars, LV, external lateral view; 17. *Candona* sp., possible juvenile of *Candona neglecta* Sars, RV, external lateral view; 18, 19. *Hydrobia syrmica* Neumayr.

Figure S3

1-4. *Ammonia beccarii* (Linné); 5-9. *Cyprideis torosa* (Jones); 5, 6. LV, lateral external view; 7. RV, external lateral view, male; 8, 9. RV, external lateral view, females; 10-14. *Loxoconcha laevatula* Livental; 10,11. RV, lateral external view, males; 12, 13. RV, lateral external view, femals; 14, RV, internal view, female; 15, 16. *Amnicythere gubkini* Livental; 15. LV, external lateral view; 16. RV, external lateral view; 17, 18. *Hydrobia syrmica* Neumayr.

Figure S4

1-7. *Cyprideis torosa* (Jones),with smooth shell, forma *littoralis*; 1. LV, external lateral view, male; 2. RV, external lateral view, male; 3, 5. Carapace, lateral view from the RV, female; 4. LV, external lateral view, female; 6. LV, internal view, female; 7. Crapace, dorsal view; 8-15. *Loxoconcha eichwaldi* Livental var. *tuberculata*; 8. LV, external lateral view, male; 9. RV, external lateral view, male; 10. Carapace, lateral view from RV, male; 11. LV, , external lateral view, female; 12. Carapace, lateral view from RV, female; 13. LV, internal view, female; 14. Carapace, dorsal view, female; 15. Carapace, ventral view, female; 16-21. *Loxoconcha petasus* Livental; 16. LV, external lateral view, male; 17, 18. RV, external lateral view, male; 19. LV, extenal lateral view, female; 20. RV, external alteral view, female; 21. RV, internal view, male; 22-25. *Loxoconcha* ex. gr. *eichwaldi* Livental; 22. LV, external lateral view, male; 23. RV, external lateral view, male; 24. LV, external lateral view, female; 25. RV, external lateral view, female; 26-31. *Amnicythere* ex. gr. *gubkini* Livental; 26, 28. LV, external lateral view; 27. RV, external lateral view; 29. Carapace, view from the RV; 30. Carapace, dorsal view; 31, Carapace, ventral view; 32, 33. *Candona* ex. gr. *angulata* G. W. Müller; 32.Carapace, lateral view

from the LV, male; 33. Carapace, lateral view from the RV, male; 34, 35. *Hydrobia* ex. gr *syrmica* Neumayr.

References

AGALAROVA, D.A., KADYROVA, Z.K. & KULIEVA, S.A. (1961) *Ostracoda from Pliocene and Post-Pliocene Deposits of Azerbaijan (in Russian).* Azerbaijan State Publisher, Baku.

GOFMAN, E.A. (1966) *Ecology of Modern and Novocaspian Ostracods of the Caspian Sea (in Russian).* Akademie NAUK SSSR, Moscow.

SCHORNIKOV, E.I. (1964) Opyt Vydelenija Kaspiïskikh Elementov Fauny Ostrakod V Azovo-Tchernomorskom Basseïne (an Experiment on the Distinction of the Caspian Elements of the Ostracod Fauna in the Azov – Black Sea Basin) (in Russian). *Zoologitcheskiï zhournal*, **63,** 1276-1293.

VAN BAAK, C.G.C., VASILIEV, I., STOICA, M., KUIPER, K.F., FORTE, A.M., ALIYEVA, E. & KRIJGSMAN, W. (2013) A Magnetostratigraphic Time Frame for Plio-Pleistocene Transgressions in the South Caspian Basin, Azerbaijan. *Global and Planetary Change*, **103,** 119-134.

VEKUA, M.L. (1975) *Ostracods from the Kimmerian and Kujalnikian Deposits of Abkasia and Their Stratigraphic Importance (in Russian).* Academie Nauk Gorjistan SSR.

YASSINI, I. (1986) Ecology, Paleoecology and Stratigraphy of Ostracods from Late Pliocene and Quaternary Deposits of the South Caspian Sea Region in North Iran. In: *Shallow Tethys 2* (Ed. by K. H. McKenzie), 475-497.

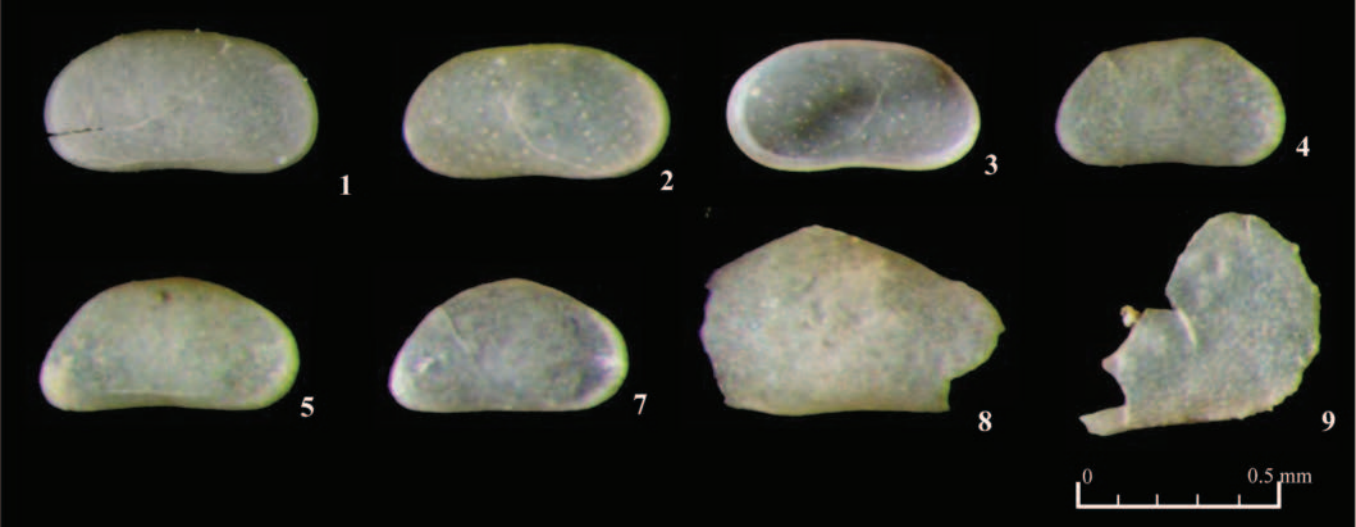
1
2
3
4
5
7
8
9
0
0.5 mm

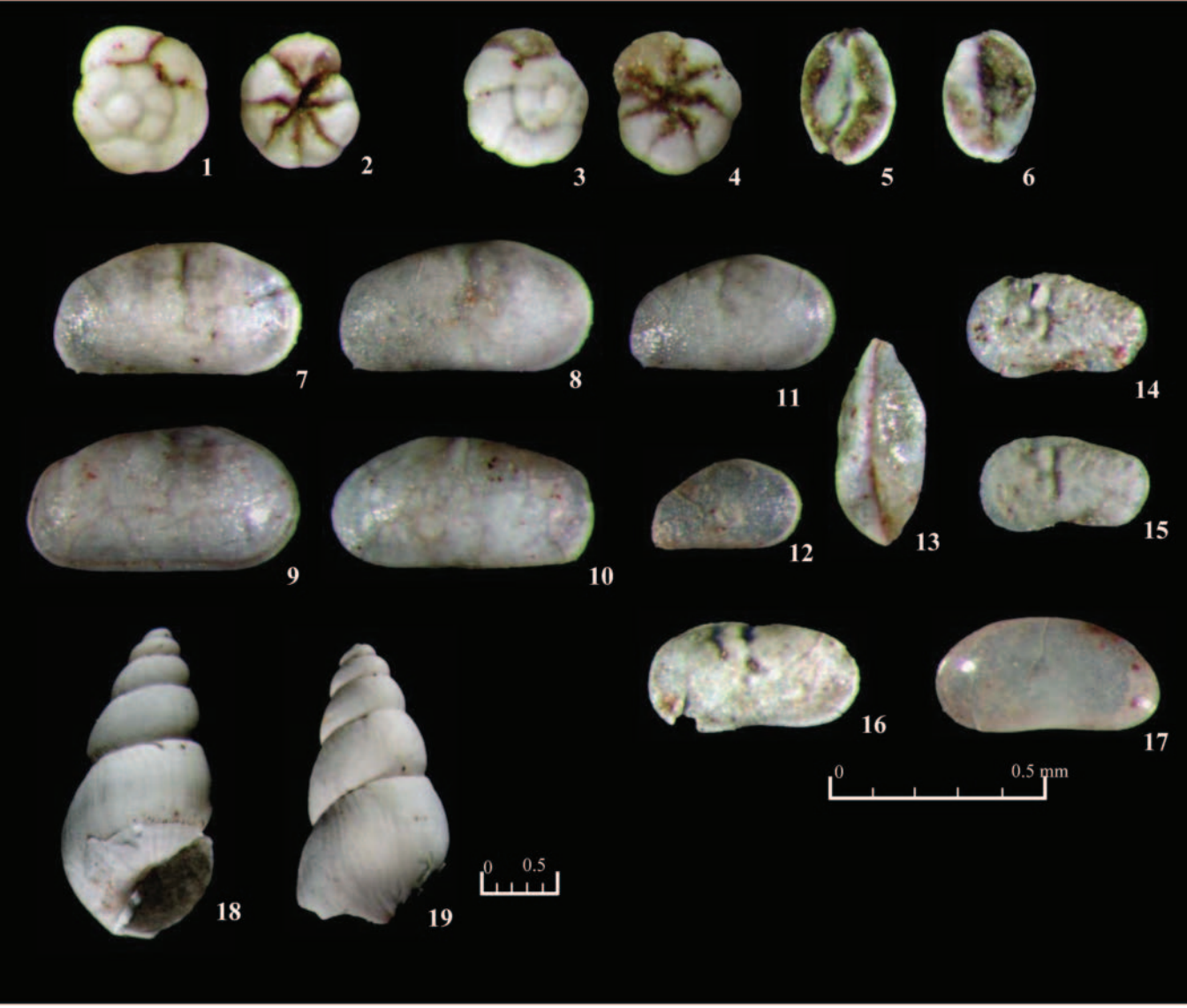
1
2
3
4
5
6
7
8
11
14
9
10
12
13
15
16
17
0
0.5 mm
18
19
0
0.5

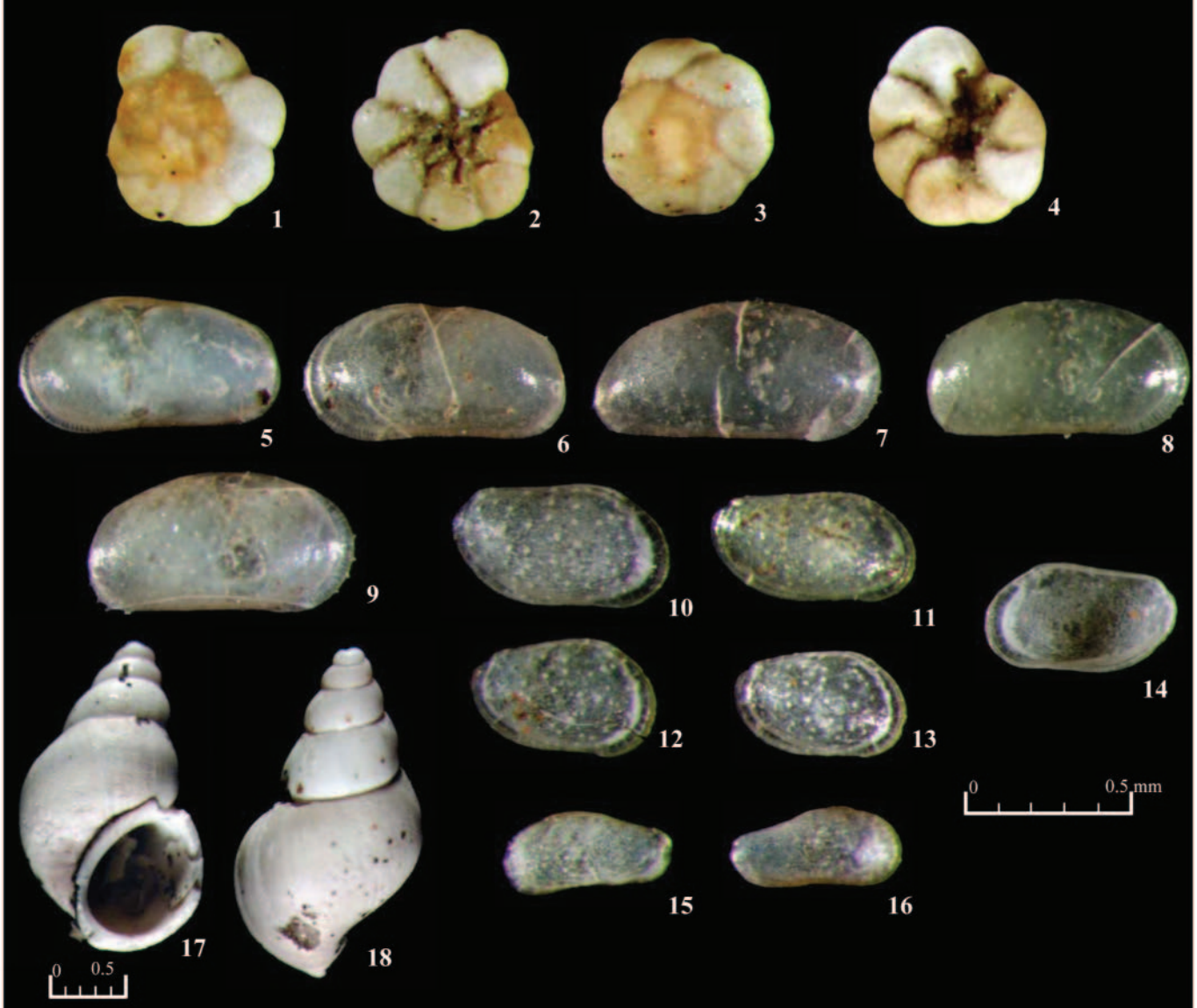
1
2
3
4
5
6
7
8
9
10
11
12
13
14
0
0.5 mm
15
16
17
18
0
0.5


1
2
3
4
5
6
7
8
9
10
11
12
13
14
15
16
17
18
22
23
19
20
21
24
25
26
27
28
29
30
31
32
33
34
35
0
0.5 mm
0
0.5